RESEARCH ARTICLE | OPEN ACCESS

Single Cell Deletion of the Transcription Factors Trps1 and Sox9 in Astrocytes Reveals Novel Functions in the Adult Cerebral Cortex

Poornemaa Natarajan[1,2,3,4] | Christina Koupourtidou[2,3,5] | Thibault de Resseguier[1] | Manja Thorwirth[1,2] | Riccardo Bocchi[1,2] | Judith Fischer-Sternjak[1,2] | Sarah Gleiss[1] | Diana Rodrigues[1,5] | Michael H. Myoga[1,5] | Jovica Ninkovic[2,6,7] | Giacomo Masserdotti[1,2] | Magdalena Götz[1,2,7]

[1]Biomedical Center Munich, Department of Physiological Genomics, LMU Munich, Martinsried, Germany | [2]Institute for Stem Cell Research, Helmholtz Center Munich, German Research Center for Environmental Health (GmbH), Neuherberg, Germany | [3]Graduate School of Systemic Neurosciences, Biocenter, Martinsried, Germany | [4]Max-Planck-Institute for Biochemistry, International Max Planck Research School for Life Sciences, Munich, Germany | [5]Max Planck Institute for Biological Intelligence, Martinsried, Germany | [6]Biomedical Center Munich, Department of Cell Biology and Anatomy, LMU Munich, Martinsried, Germany | [7]Excellence Cluster of Systems Neurology (SYNERGY), Munich, Germany

Correspondence: Magdalena Götz (magdalena.goetz@bmc.med.lmu.de)

ABSTRACT

Astrocytes play key roles in brain function, but how these are orchestrated by transcription factors (TFs) in the adult brain and aligned with astrocyte heterogeneity is largely unknown. Here we examined the localization and function of the novel astrocyte TF Trps1 (Transcriptional Repressor GATA Binding 1) and the well-known astrocyte TF Sox9 by Cas9-mediated deletion using Mokola-pseudotyped lentiviral delivery into the adult cerebral cortex. Trps1 and Sox9 levels showed heterogeneity among adult cortical astrocytes, which prompted us to explore the effects of deleting either Sox9 or Trps1 alone or simultaneously at the single-cell (by patch-based single-cell transcriptomics) and tissue levels (by spatial transcriptomics). This revealed TF-specific functions in astrocytes, such as synapse maintenance with the strongest effects on synapse number achieved by Trps1 deletion and a common effect on immune response. In addition, spatial transcriptomics showed non-cell-autonomous effects on the surrounding cells, such as oligodendrocytes and other immune cells with TF-specific differences on the type of immune cells: Trps1 deletion affecting monocytes specifically, while Sox9 deletion acting mostly on microglia and deletion of both TF affecting mostly B cells. Taken together, this study reveals novel roles of Trps1 and Sox9 in adult astrocytes and their communication with other glial and immune cells.

1 | Introduction

Astrocytes are integral to numerous functions throughout the central nervous system. While the importance of transcription factors (TFs) is well documented in astrocyte fate specification during development (Kang et al. 2012; Tiwari et al. 2018), their roles in mature astrocytes and their involvement in astrocyte heterogeneity are largely elusive. For example, the TFs Sox9, Nfia, and Nfib have been implicated in astrocyte specification (Deneen et al. 2006; Kang et al. 2012; Klum et al. 2018) and

---

Giacomo Masserdotti and Magdalena Götz contributed equally.

are still rather ubiquitously expressed in adult astrocytes (Sun et al. 2017). Such pan-astrocyte TFs play unique and region-specific roles in astrocytes during postnatal development (Cheng et al. 2023), in the intact adult brain (Huang et al. 2020; Ung et al. 2021), in response to injury (Laug et al. 2019) or in disease (Glasgow et al. 2017; Sardar et al. 2022). Interestingly, Sox9 was shown to have a role only in specific brain regions, while no role for Sox9 has been discovered yet in the cerebral cortex (Cheng et al. 2023; Ung et al. 2021).

We therefore set out to explore the function of Sox9 in adult cortical gray matter (GM) astrocytes at the single-cell level, thereby considering possible cellular heterogeneity. We further aimed to determine the role of a novel adult astrocyte TF, Trps1 (Transcriptional Repressor GATA Binding 1 or Tricho-Rhino-Phalangeal Syndrome Type I). Its expression has been detected in adult astrocytes (Endo et al. 2022; Ohlig et al. 2021; Sirko et al. 2015) and Trps1 and Sox9 are involved in similar transcriptional cascades in other cell types, such as chondrocytes or hair follicle epithelial cells (Fantauzzo et al. 2012; Tan et al. 2018). Trps1 was also predicted to be a TF driving both astrocyte and oligodendrocyte fate during development (Weng et al. 2019), but its protein localization in specific cell types, expression levels, and function have not been examined in the brain.

Importantly, no single cell deletion analysis has been performed for any TF in astrocytes, despite their known heterogeneity within and across brain regions (Bayraktar et al. 2020; Endo et al. 2022; Lanjakornsiripan et al. 2018; Ohlig et al. 2021). Here, we characterized the protein levels of Sox9 and Trps1 in the adult mouse cortex GM, revealing a remarkable heterogeneity and thus, raising the question of their function at single cell level. To tackle this, we deleted Sox9 and Trps1 either alone or together using a Cas9-mediated strategy, targeting specifically astrocytes by pseudotyped lentiviruses and analyzed the effects by patch-based single-cell RNA-sequencing (scRNA-seq). This revealed TF-dependent alterations related to specific astrocyte functions, such as regulation of synapse function and immune reaction. As these changes pointed to non-cell-autonomous functions, we also performed spatial transcriptomics (10xGenomics Visium, stRNA-seq) in control and single- or double-TF-deleted conditions, which revealed unexpected effects of astrocyte-specific TF deletion in their surrounding onto other cell types, such as oligodendrocytes as well as different cells of the immune system, thus supporting the patch-based scRNA-seq analysis. Notably, Sox9 and Trps1 seem to act often antagonistic, with the double deletion abolishing effects of the single deletions. Thus, Sox9 and Trps1 are involved in several functions of mature cortical astrocytes with widespread gene expression changes upon their loss, placing them at the nexus of astrocyte-mediated homeostasis.

2 | Materials and Methods

2.1 | Animals

To characterize the expression of Sox9 and Trps1 in the adult cortical GM by immunostaining, 2–5-month-old C57BL/6J mice (Charles River Laboratories; Sulzfeld, Germany) were used.

R26-Cas9-Fezh mice (Platt et al. 2014, Jackson Laboratories; Gt(ROSA)26Sortm1.1(CAG-cas9*,-EGFP) Fezh/J, JAX stock #024858) expressing Cas9-GFP in all cells constitutively were used for Sox9, Trps1 deletion experiments. Animals were bred as homozygotes and housed under specified pathogen-free conditions and a 12:12 h light/dark cycle, with 2–3 adult animals per filter top cages. All experimental procedures were performed in accordance with animal welfare policies and approved by the regional authority (Regierung von Oberbayern, Germany).

2.2 | gRNA Cloning and Viral Vector Preparation

For cloning multiple gRNAs targeting the TFs, we used the STAgR approach (Breunig et al. 2018). In brief, the gRNA-insert and gRNA-vector fragments were generated by PCR with gRNA-scaffold-Fwd and gRNA(rev)-hU6-Rev primers (see Resources Table) as described in (Breunig et al. 2018). The PCR-amplified gRNA-insert and gRNA-vector fragments were purified using AMPure XP Beads and assembled into a 2X-STAgR or 4X-STAgR construct by use of Gibson assembly (Gibson 2011). The assembled fragments were transformed into chemically competent TOP10 *Escherichia coli* bacteria and gRNA positive clones were selected by colony PCR and the isolated plasmids were further verified by Sanger sequencing using StAgR_seq_fwd2 and StAgR_seq_rev primers. The gRNA sequences were further sub-cloned into a lentiviral construct as follows: gRNA containing sequences were cut out from the STAgR plasmids by KpnI or AfeI+BsrBI digestion and ligated into a similarly generated lentiviral sticky or blunt end fragment (LTR-CMV-tdTomato-WPRE-LTR) using T4 DNA ligase (incubated at 16°C overnight) and transformed into chemically competent TOP10 *E. coli* bacteria. gRNA positive clones were selected by colony PCR and further verified by Sanger sequencing using either of the following primers: lentiSeq_fwd,_StAgR_seq_fwd2, seqWPRE_Fwd, STAGRseq_pLKOI_rev. The final assembled lentiviral constructs are as depicted in Figure 2A.

The lentiviral production was carried out as described by Heinrich et al. 2014, with the following differences. The gRNA lentiviral plasmids were transfected into HEK293T cells along with the pMokola-G plasmid (for pseudotyping) and pCM-VdR8.91 packaging plasmid. The viral particles were harvested from the medium 4 days later. The media was collected in 50 mL tubes, spun down at 3500 rpm for 5 min, and filtered with a 0.45 μm filter into a conical-bottom ultracentrifuge tube containing OptiPrep. After ultracentrifugation at 24,000 rpm for 2 h, most of the supernatant was removed without disturbing the OptiPrep interface, re-suspended thoroughly in cold TBS-5 buffer (now ensuring complete mixing with OptiPrep), and subsequently subjected to a second round of ultracentrifugation at 24,000 rpm for 2 h. After discarding the supernatant, the viral pellet was re-suspended in an appropriate volume of TBS-5 buffer and stored at −80°C until further use. The titer of the Mok-LVs was determined by infecting primary astrocyte cultures with serial dilutions of the concentrated viral stock: the titer was calculated based on the number of cells expressing tdTomato 3 days after transduction, expressed as titer units per milliliter (TU/ml).

The gRNA sequences and primer sequences are:

gRNA sequences	
g-Control (non-targeting sequence)	GCTGCATGGGGCGCGAATCA
g-Sox9_exon1	GTACCCGCATCTGCACAACG
g-Sox9_exon2	GCTGGTACTTGTAATCGGGG
g-Trps1_exon1	TAGGACTGCATAATCGCACC
g-Trps1_exon3	AGAGGGGCAGACATCCTACG
Primers for gRNA cloning	
g-Sox9_exon1_Scaffold-fwd	GTACCCGCATCTGCACAACGGTTTTAGAGCTAGAAATAGCAAGTT
g-Sox9_exon1_hU6_Rev	CGTTGTGCAGATGCGGGTACCGGTGTTTCGTCCTTT
g-Sox9_exon2_Scaffold-fwd	GCTGGTACTTGTAATCGGGGGTTTTAGAGCTAGAAATAGCAAGTT
g-Sox9_exon2_hU6_Rev	CCCCGATTACAAGTACCAGCCGGTGTTTCGTCCTTT
g-Trps1_exon1_Scaffold_fwd	TAGGACTGCATAATCGCACCGTTTTAGAGCTAGAAATAGCAAGTT
g-Trps1_exon1_hU6_Rev	GGTGCGATTATGCAGTCCTACGGTGTTTCGTCCTTT
g-Trps1_exon3_Scaffold_fwd	AGAGGGGCAGACATCCTACGGTTTTAGAGCTAGAAATAGCAAGTT
g-Trps1_exon3_hU6_Rev	CGTAGGATGTCTGCCCCTCTCGGTGTTTCGTCCTTT
g-Control_Scaffold-fwd	GCTGCATGGGGCGCGAATCAGTTTTAGAGCTAGAAATAGCAAGTT
g-Control_hU6_Rev	TGATTCGCGCCCCATGCAGCCGGTGTTTCGTCCTTT
Primers for Sanger sequencing	
StAgR_seq_fwd2	ACTGGATCCGGTACCAAGG
StAgR_seq_rev	TTACGGTTCCTGGCCTTTTG
STAGRseq_pLKOI_rev	ACCAATGACTTACAAGGCAGC
seqWPRE_Fwd	TCCTTCTGCTACGTCCCTTC
lentiSeq_fwd	ATCGTTTCAGACCCACCTCC

2.3 | Viral Injection in R26-Cas9-Fezh Mice

Adult (2–4 months old) animals homozygous for Cas9 were used for lentiviral injection to achieve CRISPR-mediated deletion of astrocyte TFs. Briefly, animals were anesthetized and injected with the Mok-LV virus at a titer of $1–5 \times 10^8$ TU/ml in one hemisphere, Bregma: RC: −0.4 to −1.4 mm; ML: −1.0 mm; DV: −0.65 mm. The animals were killed 7 or 21 days after the Mok-LV injection by transcardial perfusion with phosphate-buffered saline (PBS), followed by 4% paraformaldehyde (PFA) in PBS. The brains from these animals were removed and post-fixed for 24 h in 4% PFA, following which the 40 μm thick sections were cut at the vibratome and the brain slices were stored in PBS with sodium azide at 4°C until further analysis by immunostainings. The animals used for Sox9 and Trps1 characterization by immunostainings were perfused and processed in a similar manner, but without any viral injections.

2.4 | Immunohistochemistry

For immunohistology, sections, stored in 1XPBS with sodium azide, were washed with 1XPBS three times for 10 min each; then, they were pre-incubated for 90 min in blocking solution (3% bovine serum albumin, 0.5% Triton X-100 in 1XPBS). Primary antibodies were diluted in blocking solution (as mentioned in the Resources Table); the sections were incubated with the appropriate antibody combination for 48 h at 4°C. Then, the slices were washed with 1XPBS three times, 10 min each washing. Then, slices were incubated for 2 h with the appropriate species- or subclass-specific secondary antibodies and 4′,6-diamidino-2-phenylindole (DAPI, to label the nuclei) diluted in blocking solution. After washing the slices in 1XPBS for three times, they were mounted with Aqua Poly/Mount (Polysciences, Warrington, PA). For Trps1, synaptophysin, and Homer1 immunostainings, antigen retrieval steps with 0.01 M Sodium citrate (pH 6) at 90°C for 20 min was performed before incubation with the corresponding primary antibodies. The following primary and secondary antibodies were used at the mentioned dilutions:

Primary antibody	Dilution	Company/ catalogue number
Rabbit anti-Sox9	1:1500	Merck/Millipore (AB5535)
Rabbit anti-Trps1	1:300	Abcam (ab209664)

Primary antibody	Dilution	Company/ catalogue number
Mouse IgG1 anti-S100β	1:300	Sigma (S2532)
Goat anti-Sox9	1:500	AF3075-SP
Mouse IgG1 anti-Gfap	1:300	Sigma (G3893)
Mouse IgG1 anti-Synaptophysin	1:500	Synaptic Systems (SYSY101011)
Rabbit anti-Homer1	1:500	Synaptic systems (SYSY 160003)
Goat anti-mcherry	1:1000	Acris/Origene (AB0081-200)
Rabbit anti-RFP	1:1000	Rockland (600–401-379)
Mouse IgG2a anti-Olig2	1:250	Merck/Millipore (MABN50)
Rat IgG2a BrdU	1:300	Abcam (AB6326)
Rabbit Bcas1	1: 500	SYSY 445003

Secondary antibody	Dilution	Company/ catalogue number
Donkey anti-mouse IgG A488	1:250	Life Technologies (A21202)
Donkey anti-goat A594	1:1000	Life Technologies (A-11058)
Donkey anti-rabbit Cy3	1:1000	Dianova, 711-165-152
Donkey anti-Rabbit IgG Alexa Fluor 647	1:1000	Jackson (Biozol) JIM-711-165-152
Goat anti-mouse IgG1 Alexa Fluor 488	1:1000	Life Technologies (A21121)
Goat anti-Mouse IgG2a Antibody, Alexa Fluor 647	1:1000	Invitrogen A21241
Goat anti-Rabbit IgG (H+L) A405	1:250	ThermoFisher (A-31556)
DAPI (nuclear staining)	1:1000 (0.1 μg/mL)	Sigma, D9564

2.5 | Quantification and Statistical Analysis for Immunohistochemistry

Images were obtained using a Confocal laser scanning (Zeiss LSM710) microscope and analyzed using ImageJ or Imaris (for synapse analysis). Images for Sox9 and Trps1 characterization in the adult cortex were taken as a tiled image at a magnification of 25X to cover the entire cortical column in the somatosensory cortex area, with 12–20μm thick z stacks. The proportion of Sox9 or Trps1 positive (or double-positive cells) was obtained by counting all the S100β+ astrocytes or Olig2+ oligodendroglial lineage cells. To understand the layer distribution, the cortical GM was divided into five equal bins, with bins 1, 2 corresponding to the upper cortical layers and bin 3 in the middle and bins 4 and 5 corresponding to the deeper cortical layers. The intensity of Sox9 and Trps1 was calculated for all the cells in the cortical column, based on ROIs drawn for DAPI signal. A cell was considered positive for Sox9 or Trps1 if the normalized corrected total cell fluorescence was more than 0.3 and 0.15, respectively. Images for validation of Sox9, Trps1 deletion after Mok-LV injection were taken as tiled images at a magnification of 25X to cover the entire region of injection along the cortical column, with 12–20μm thick z stacks. The proportion of infected cells (tdTomato+) cells expressing Sox9, Trps1, S100β, or Gfap was expressed as a percentage of gRNA-tdTomato+ cells.

Confocal images for synaptic puncta analysis were taken at a magnification of ×40 (with a ×2.5 zoom) with 4.5–7μm thick z stacks. Each image contained 1–3 infected astrocytes, and at least five ROIs were imaged for each animal. The images were deconvolved and the astrocyte surface was reconstructed (based on the signal for tdTomato, i.e., gRNA infected astrocytes or Aldh1l1-eGFP; see, e.g., Figures 4D1′–F1′ and S6I1′,J1′) on Imaris. Following this, the number of pre- and post-synaptic puncta in the regions surrounding the astrocyte (within a distance of 0–1.5μm from the astrocyte surface) were calculated with the "Spots" function on Imaris (see, e.g., Figures 4D2′,D3′,E2′,E3′,F2′,F3′ and S6F2′,F3′,I2′,I3′, J2′, J3′). Synapses were defined as post-synaptic puncta located within 0–0.2μm of the closest pre-synaptic puncta, a distance threshold that reflects the typical synaptic cleft size of ~20–30 nm (e.g., see Figures 4D4,E4,F4 and S6F4,I4,J4). The synapse numbers were normalized to the volume of the reconstructed astrocyte surface and represented as a Fold-change to the average of the g-Control condition in each batch of the experiment.

All statistical tests were performed with GraphPad Prism 9.5. Parametric One-way ANOVA with Tukey's test for comparison was performed if all the conditions in a comparison passed Shapiro–Wilk test for normality. Otherwise Kruskal-Wallis test with Dunn's test for multiple comparisons was performed. The exact test used for each graph is also mentioned in the corresponding figure legends, all barplots are represented as mean±SEM. Data in the figures are available at: https://doi.org/10.5281/zenodo.14065517.

2.6 | Patch-Based scRNA-Seq (Patch-Seq)

Smart-seq2 based Patch-seq of astrocytes was performed using a modified version of the protocol established for neurons (Cadwell et al. 2017; Cadwell et al. 2016). Briefly, acute cortical slices of 300μm thickness were obtained from animals injected with g-Control, g-Sox9, g-Trps1, or g-Sox9+ Trps1 Mok-LVs. At 7 or 21dpi, mice were decapitated and brain were rapidly removed and placed in oxygenated N-methyl-D-glucamine-based (NMDG) artificial cerebrospinal fluid (aCSF) solution containing the following (mM): 135 NMDG, 1.5 KCl, 1.5 KH$_2$PO$_4$, 25 choline-bicarbonate, 25 glucose, 0.4 ascorbic acid, 0.5 CaCl$_2$

and 3.5 MgCl$_2$ (pH 7.2–7.4, 300–310 mOsm). The brain slices were cut using a vibratome (Leica Microsystems, VT1200S) and then incubated for 30 min at 37°C ± 0.5°C in an oxygenated aCSF solution containing the following (in mM): 125 NaCl, 2.5 KCl, 1 glucose 1.25 NaH$_2$PO$_4$, 1 glucose,2 CaCl$_2$ and 2 MgCl$_2$ (7.2–7.4 pH, 300–310 mOsm). The infected astrocytes (identified based on the signal for tdTomato in the Mok-LV construct) were collected using a patch-clamp pipette and immediately transferred to individual tubes containing a lysis buffer based on (Cadwell et al. 2017). Subsequent reverse-transcription and cDNA amplification steps were carried out using Superscript II Reverse Transcriptase (SSIIRT; Thermo Fisher Scientific, cat. no. 18064014) and KAPA Biosystems HiFi HotStart Ready Mix (Thermo Fisher Scientific, cat. no. NC0295239), respectively. The generated cDNA was purified with Axygen AxyPrep mag PCR clean-up kit (Thermo Fisher Scientific, cat. no. 14223151) using a ratio of 0.6:1 (vol beads to vol PCR reaction) and the purified cDNA was checked by running 1 μL of the sample on an Agilent Bioanalyzer or Qubit (Thermo Fisher), as per manufacturer's instructions. Samples with good quality cDNA (based on assessments in Cadwell et al. 2017) were sent to the Laboratory for Functional Genome Analysis (LAFUGA) at the Gene Center Munich, where further downstream steps such as tagmentation reaction and sequencing were carried out, similar to (Cadwell et al. 2017). After sequencing, raw reads were de-multiplexed on an in-house high-performance-cluster (HPC) using Je (version 2.0.2). The raw sequencing reads were aligned to the Ensembl GRCm38 mouse reference genome using STAR aligner (version 2.7.1) with the GeneCounts parameter activated. See subsection "Data analysis for scRNA-seq of cortical GM astrocytes, Patch-based scRNA-seq (Patch-seq) and stRNA-seq" for details about subsequent data analysis of these data. Data are available at Gene Omnibus (GEO) ID: GSE279676.

2.7 | In Situ Hybridization

RNA in situ hybridization was performed using RNAscope Multiplex Fluorescent Reagent Kit (ACD, 323110) according to the manufacturer's instructions. Briefly, brain sections were fixed in 4% paraformaldehyde at 4°C for 15 min, ethanol-dehydrated (Carl Roth #9065.4), treated with H$_2$O$_2$ (ACD, 322381) and protease-permeabilized for 20 min at 40°C. Brain sections were then incubated for 2 h at 40°C using the following probes: *Serpina3n* (ACD, 430191-C2) and *Cxcl10* (ACD, 408921-C3). Signal was amplified according to the manufacturer's instructions (user manual Cat. No.: 320293, Fluorophore Opal 520: Akoya Biosciences FP1488001KT and Opal 690: Akoya FP1497001KT). Subsequently, sections were processed with immunohistochemistry analysis as described above. The primary antibody used in combination with RNAscope was rabbit antibody to RFP (1:500) to detect gRNA-infected astrocytes (tdTomato). The slices were stored at −20°C until imaging was carried out either with an inverted Leica SP8 microscope using the LASX software (Leica) at the core facility bioimaging of the Biomedical Center (BMC) or Confocal laser scanning (Zeiss LSM710) microscope. Images were acquired at a magnification of ×40 (with a ×2 zoom) with 4.5–7 μm thick z-stacks. The images were analyzed using ImageJ; the number of *Serpina3n* and *Cxcl10* puncta were counted within the area thresholded for the signal of tdTomato (gRNA-infected astrocytes). The statistics

for comparison was performed with GraphPad Prism 9.5, where Kruskal-Wallis test and Dunn's test for multiple comparisons were performed.

2.8 | Spatial Transcriptomics (stRNA-Seq) Analysis

Animals injected with Mok-LV gRNAs were sacrificed at 7dpi; the extracted brains were embedded and snap-frozen in an isopentane and liquid nitrogen bath as recommended by 10xGenomics (Protocol: CG000240). The brains were resected to generate smaller samples (as shown in Figure 5B) at the cryostat (Thermo Scientific CryoStar NX50) and 10 μm thick coronal sections of the dorsal brain were cut. The sections were checked for the presence of infected cells (tdTomato+ cells) briefly. After confirming that we were at the region of injection, two consecutive 10 μm thick sections containing infected cells were placed in one capture area each. The tissue was stained using H&E staining and imaged with the Carl Zeiss Axio Imager.M2m microscope using ×10 objective (Protocol: CG0001600). The libraries were prepared with Visium Spatial Gene Expression Reagent Kits (CG000239) with 18 min permeabilization time and sequenced on an Illumina HiSeq1500 instrument and a paired-end flowcell (High output) according to manufacturer protocol. Sequencing was performed in the Laboratory for Functional Genome Analysis (LAFUGA). Data were mapped against the mouse reference genome mm10 (GENCODE vM23/Ensembl 98; build versions 1.2.0 and 2020A from 10xGenomics) with Space Ranger 1.2.2. Further downstream analysis of this data was performed in RStudio (Posit PBC) using the Seurat and Bioconductor packages. For quality control, only spots with less than 30% mitochondrial reads, less than 20% hemoglobin reads, and at least 250 detectable genes were selected for further analysis. The four samples were merged on Seurat and spots specific to the cortical GM were selected based on the anatomical position. Data were analyzed as explained below. Data are available at Gene Omnibus (GEO) ID: GSE279677.

2.9 | Data Analysis for scRNA-Seq of Cortical GM Astrocytes, Patch-Seq Based scRNA-Seq and stRNA-Seq

All the scRNA-seq and stRNA-seq data were analyzed on RStudio, using packages from Bioconductor and Seurat and the GO analysis was performed with the enrichGO function and simplified with the Rrvgo package to avoid redundant GO terms. scRNA-seq for cortical GM astrocytes (10xGenomics) was kindly provided by Bocchi et al. (in revision/accepted in principle). Cells annotated as cortical GM astrocytes in this dataset were selected for downstream analysis, which resulted in 3150 cells. "FindClusters" function was used at a resolution of 0.5 and this gave rise to six clusters with distinct gene expression patterns. For Patch-seq-based scRNA-seq data and stRNA-seq data, the cells were clustered with a resolution of 0.8. For comparison of our stRNA-seq data with response after SWI, we used the scRNA-seq data set (10xGenomics) for cells from cortical GM at 5dpSWI (Koupourtidou et al. 2024). The module scores for each of the annotated cell type were calculated based on the top 25 DEGs using the AddModulescore function in Seurat.

2.10 | Other Resources

Software and algorithms

Resource	Identifier
ImageJ	https://imagej.net/Downloads
Imaris 9.7.2	Access to software provided by Core Facility Bioimaging, Biomedical Center, LMU (https://imaris.oxinst.com/)
ZEN software, Zeiss	https://www.zeiss.com/microscopy/en_us/products/microscope software/zen.html
Microsoft Excel	https://www.microsoft.com/en-gb/
GraphPad Prism 9.5	https://www.graphpad.com/
Affinity Designer 1.1	https://affinity.serif.com/en-us/designer/
RStudio	https://rstudio.com
R ggplot2	https://ggplot2.tidyverse.org
Seurat (v4.3)	https://github.com/satijalab/seurat/blob/HEAD/vignettes/install.Rmd
enrichGO (ClusterProfiler)	https://bioconductor.org/packages/release/bioc/vignettes/clusterProfiler/inst/doc/clusterProfiler.html
Rrvgo	https://www.micropublication.org/journals/biology/micropub-biology-000811

3 | Results

3.1 | Adult Murine Cortical Astrocytes Show Heterogeneity in Trps1 and Sox9 Levels

As Trps1 has been detected in astrocytes by several RNA-seq studies, we first examined its protein levels along with Sox9 and S100β (as a general marker for astrocytes) in the cerebral cortex of young adult 2–3 months old mice (Figure 1A,B). First, we monitored the distribution of immunopositive cells across a column of the cortex GM, divided into five equal bins (Figure 1C), and quantified the percentage Sox9+S100β+ or Trps1+ S100β+ astrocytes per bin (Figure 1D,E). Most S100β astrocytes were positive for Sox9 (76%, Figure 1F) and this was not significantly different across the cortical layers (Figure 1D). Conversely, only 40% of the S100β+ astrocytes were positive for Trps1, most of

which were also Sox9+ (Figure 1F). We also observed a trend toward higher proportions of S100β− Trps1 double positive astrocytes in upper compared to lower bins (Figure 1E). While all the Sox9+ cells in the cortical GM were positive for S100β and, hence, astrocytes (Figure S1A), only 35.5% of Trps1+ cells were S100β+ or Sox9+, suggesting that Trps1 may also label other glial cells (Figure S1B). Therefore, we stained for Trps1, Olig2, and S100β and found 50% of the Olig2 positive oligodendroglial lineage cells to be Trps1+ (Figure S1C). Conversely, 63% of Trps1+ cells were Olig2+, and 11% were S100β+(together or without Olig2; Figure S1D). These data suggest that Trps1 is expressed in both astrocyte and oligodendrocyte lineage in the adult brain, similar to the developing brain (Weng et al. 2019).

Next, we evaluated the expression of the proteins Sox9 and Trps1 by measuring the fluorescence intensity of all the cells within each bin of the cortical column. The normalized corrected total cell fluorescence (CTCF) for either Sox9 or Trps1 showed remarkable heterogeneity (as observed in the color-coded dot plot; Figure 1C). The fluorescence intensity of all the Sox9+ cells did not show considerable variation across bins (Figure 1G). However, the cells positive for both Sox9 and Trps1 had higher levels of Sox9 signal (in bins 2–5, with significantly higher levels in bins 3 and 4). Conversely, Trps1 seems lower in Sox9-Trps1 double positive cells compared to Trps1-only positive cells (Figure 1H, in bins 2–5, with significantly lower levels in bin 5, i.e., in the deeper layers (DL)). Overall, Trps1 seems less abundant in the upper layers (UL, bin 1).

Given this heterogeneity at the protein level, we explored if this could also be detected at mRNA level, or if this is entirely posttranscriptional. Therefore, we analyzed the expression of *Sox9* and *Trps1* in scRNA-seq dataset from our lab (10xGenomics, Bocchi et al. (unpublished)) comprising cells from cortical GM and white matter (WM), taken by means of a biopsy punch without any specific selection for astrocytes. Subsetting GM astrocytes by the expression of known astrocyte genes (Astrocyte score, Figure S1E; genes shown in Table S1) resulted in 3150 cells, which were almost negative for other glial lineage-specific genes, such as *Olig2* or *Sox10* for the oligodendrocyte lineage and *Tmem119* or *Aif1* (*Iba1*) for microglia (Figure S1G). Among the six astrocyte clusters (Figure S1E,H), considerable differences in the expression levels of the 2 genes were observed: for instance, in clusters A and E both *Sox9* and *Trps1* are highly expressed, while in other clusters their expression is highly variable, with the lowest expression of *Sox9* and *Trps1* in cluster C (Figure S1F). Together, scRNA-seq analysis of astrocytes isolated from adult cortical gray matter supported the heterogeneity of Sox9 and Trps1 found at protein level.

3.2 | CRISPR Mediated Deletion of Trps1 and Sox9 in Astrocytes

Given this interesting heterogeneity, we explored the effects of Sox9 and Trps1 deletion in cortical GM astrocytes at the single-cell level. To this end, we used a CRISPR (Clustered Regularly Interspaced Short Palindromic Repeats)/Cas9 mediated strategy, delivering the respective gRNAs to astrocytes by Mokola-pseudotyped lentivirus (Mok-LV) (Watson et al. 2002)
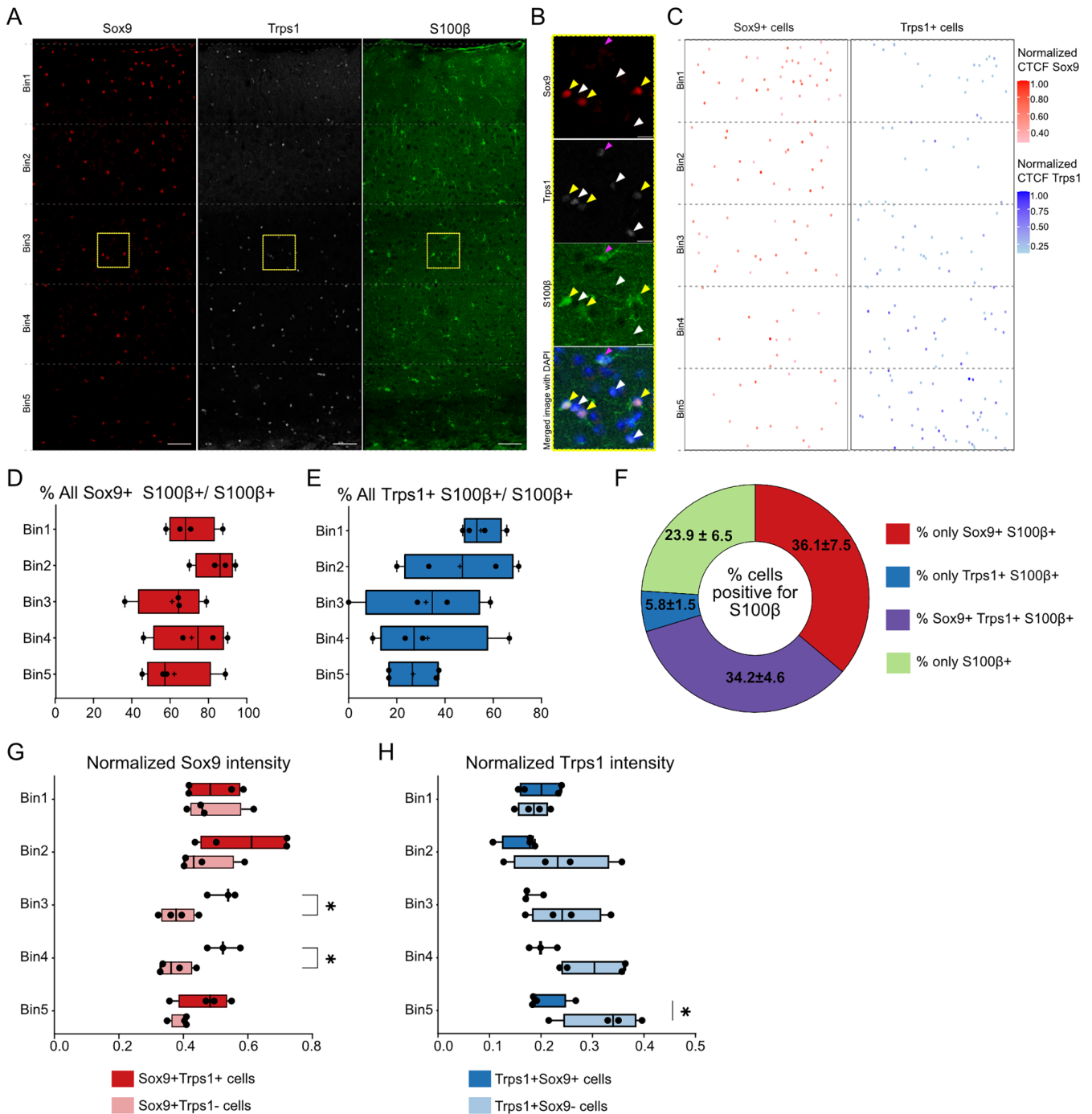
FIGURE 1 | Characterization of Trps1 and Sox9 protein in the cortical GM. (A) Micrographs of Sox9, Trps1, and S100β immunostaining in the adult murine cortex. Scale bar = 50 μm. (B) Magnification of areas highlighted in yellow boxes of the respective image in A; yellow arrowheads point to cells positive for Sox9, Trps1, and S100β; magenta arrowheads point to cells positive for Trps1 and S100β; white arrowheads point to cells positive for only Trps1. Scale bar = 10 μm. (C) Reconstruction of the distribution and intensity of Sox9 and Trps1 in a cortical column divided into 5 bins; Sox9 and Trps1 intensities are color-coded in red and blue, respectively. (D, E) Boxplots showing bin-wise percentage of S100β+ astrocytes expressing (D) Sox9 and (E) Trps1 (n biological replicates = 4; Data shown as IQR+ whiskers). (F) Percentage of Sox9 or Trps1 over S100β+ cells in the cortical GM (n biological replicates = 4, data labels indicate). Data shown as %Mean ± SEM; all cells were considered, irrespective of bins or layers. (G, H) Boxplots showing quantification for the normalized (G) Sox9 and (H) Trps1 intensity for cells positive for both Sox9+ Trps1+ cells or only Sox9+ or Trps1+ cells across bins (n biological replicates = 4. Data shown as IQR + whiskers). Statistics for comparison were analyzed by Two-way ANOVA (by fitting a mixed model or Sidak's multiple comparison test), *$p \leq 0.05$.

in transgenic mice ubiquitously expressing Cas9-GFP (Platt et al. 2014). Two gRNAs per gene, targeting different exons, were cloned in the same lentiviral vector, to increase the knockdown efficiency (Replogle et al. 2022). Furthermore, they were multiplexed (Breunig et al. 2018), thus allowing the regulation of either only Sox9, only Trps1, or Sox9 and Trps1 simultaneously, together with the coding sequence for a fluorescent reporter under a CMV promoter (Figure 2A). First, we confirmed
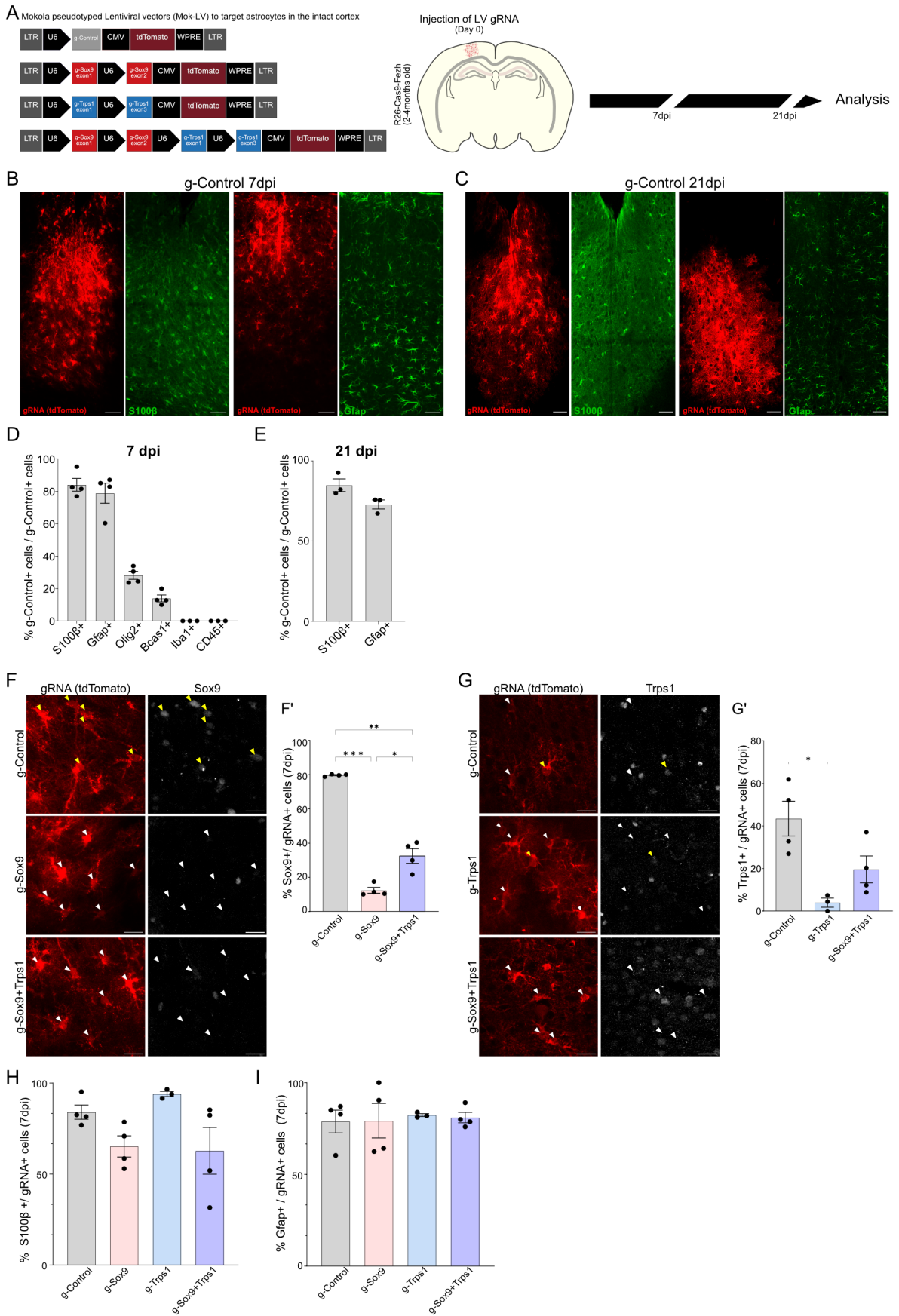
FIGURE 2 | Legend on next page.

the specificity of the virus to target astrocytes by injecting about 750 nL of the control gRNA (g-Control) Mok-LV at a titer of 10^5 infective particles per milliliter (TU/mL) into the somatosensory cortex. This resulted in a substantial number of infected cells in the injected region both at 7 or 21 days post injection (dpi, Figure 2B,C); more than 80% of the transduced cells were immunopositive for the astrocyte markers S100β or Gfap (Figure 2D,E) at both time points, while a smaller fraction of the infected cells was positive for oligodendrocyte lineage markers like Olig2 (27%) or Bcas1 (14%), but no cells were positive for Iba1 or CD45 (Figure 2D, Figure S2A). These results confirm that Mok-LV targets astrocytes with high specificity and efficiency (Watson et al. 2002).

We next injected Mok-LV expressing gRNAs against Sox9 (hereafter, g-Sox9) or Trps1 (g-Trps1) or both (g-Sox9+Trps1) and examined their protein levels in the targeted astrocytes (examples in Figure S2B–D). Animals injected with g-Sox9 or g-Sox9+Trps1 showed a significant reduction in the number of Sox9+ cells at 7dpi (Figure 2F,F′) and 21dpi (Figure S2H,J). Notably, however, the percentage of Sox9+ cells was significantly higher in the g-Sox9+Trps1 condition at the earlier time point (Figure 2F′). Likewise, a significant reduction, with almost no Trps1+ astrocytes, was found in animals injected with g-Trps1 (Figure 2G,G′; Figure S2I,K), while Trps1 levels were more variable in the g-Sox9+Trps1 injections (Figure 2G′), suggesting limitations of multiplexing. Generally, the proportion of Trps1+ astrocytes among infected cells was more variable, consistent with its expression in subsets of astrocytes.

Next, we wondered whether TF deletion would affect astrocytes' morphology or pan-astrocyte marker expression. Most astrocytes showed a normal bushy morphology independent of the experimental condition (Figure 2F,G). Although most infected cells retained S100β and Gfap protein at 7dpi (Figure 2H,I, Figure S2B–E), we observed a slight decrease of S100β+ cells over g-Sox9 cells at 7 and 21dpi (Figure S2B–E), which could suggest either the loss of some g-Sox9 astrocytes or a downregulation of S100β. Nevertheless, the overall analysis suggests that these TF are not required for the maintenance of astrocyte identity in the adult cortex GM.

3.3 | Patch-Based scRNA-Seq Reveals Changes in a Multitude of Astrocyte Functions After Deletion of Trps1 or Sox9

To examine the consequences of Trps1 or Sox9 deletion in astrocytes at the single cell level, we performed a variation of Smart-seq2-based Patch-seq of astrocytes (as in Cadwell et al. 2016;

Cadwell et al. 2017, but without physiological recording). We chose Patch-seq, despite its relatively low throughput compared with conventional FACS-sorted scRNA-seq methods, because it presents several major advantages that we believe to be crucial for answering our scientific question accurately. Conventional scRNA-seq methods require the dissociation of the tissue, which often causes physical damage and biological stress to the cells, resulting in artefactual expression changes and a bias toward specific cell subpopulations more resilient to these procedures (Porter et al. 2020). On the other hand, Patch-based scRNA-seq uses acute brain slices that are kept vital in vitro and preserve the physiological connections and activity of the cells. Additionally, the process of collecting the cells from brain slices is carried out in seconds. Thus, Patch-seq allows us to obtain a transcriptomic dataset that reflects the more "natural" transcriptome of the cells. Furthermore, Patch-based scRNA-seq allows to know the exact location of the collected cell and, therefore, pair transcriptomes with spatial context (Lipovsek et al. 2021). This is a crucial advantage in our project, since it allows us to collect individual cells directly from their location within the brain parenchyma.

For this, individual astrocytes were collected with a patch-clamp-like microelectrode in acute cortical slices of animals injected with g-Control, g-Sox9, g-Trps1 or g-Sox9+Trps1 after establishing a so-called gigaOhm seal (Figure 3A). This allowed to collect 40 g-Control, 57 g-Sox9, 45 g-Trps1, and 39 g-Sox9+Trps1 astrocytes across two time points (7 and 21dpi), over 5 biological replicates. For a systematic and comprehensive analysis, we also collected 56 astrocytes from the intact cortex (not-injected) of Aldh1l1-eGFP animals, and performed several controls, in which the patch pipette was briefly in touch with the brain slices, but no cells were approached with the microelectrode (slice-control). Among the collected slice-controls, less than half (12 samples out of 30) had sufficient RNA and passed the quality control steps (Figure S3A). After batch correction the sequenced cells were distributed among all the clusters (Figure 3B, Figure S3B), irrespective of their condition (Figure 3C, Figure S5A) or the time point (Figure S3C). Importantly, slice-controls were distributed among several clusters (ps_bc1, ps_bc2, ps_bc4; Figures 3C, S5A), excluding a specific contamination. Overall, the cells could broadly be divided into four clusters (ps_bc0, ps_bc1, ps_bc2, ps_bc4; Figure 3B). Thus, the deletion of Sox9 or Trps1 did not have major effects on cell or subtype identity, therefore allowing the examination of possible functional consequences of their deletion in astrocytes.

Astrocytes from the intact brain were distributed mainly in clusters ps_bc0, ps_bc1, and ps_bc3, revealing their heterogeneity

---

FIGURE 2 | CRISPR mediated deletion of Trps1 and Sox9 in adult cortical astrocytes. (A) Scheme for Mokola-pseudotyped lentivirus (Mok-LV) constructs expressing control gRNA (g-Control) or gRNAs against Sox9 and Trps1, injected into the adult cortex. Analysis was performed at 7 or 21 dpi. (B, C) Micrographs showing overviews of the entire cortex thickness after g-Control injection and immunostainings for the astrocyte markers S100β or GFAP at 7 and 21 dpi (scale bars = 50 μm). (D, E) Barplots showing the percentage of g-Control cells immunopositive for S100β, Gfap, Olig2, Bcas1, Iba1 or CD45 at 7 and 21 dpi (n biological replicates = 3–4 for 7 dpi; n biological replicates = 3 for 21 dpi). Data are shown as Mean ± SEM. (F, G) Micrographs showing gRNA infected cells immunostained for (F) Sox9 or (G) Trps1 at 7 dpi (yellow arrowheads point to gRNA infected cells positive for Sox9/Trps1, white arrowheads point to cells negative for Sox9/Trps1, scale = 20 μm). Bar plots in F′ or G′ show the percentage of Sox9+ or Trps1+ among gRNA infected cells at 7 dpi respectively (n biological replicates = 3–4). One-way ANOVA with Dunnet's test for multiple comparisons was performed (*$p < 0.05$, **$p < 0.01$, ***$p < 0.0005$). (H, I) Barplots showing the percentage of gRNA infected cells immunopositive for (H) S100β and (I) GFAP at 7 dpi in all conditions (n biological replicates = 4 for 7 dpi). Data are shown as Mean ± SEM.
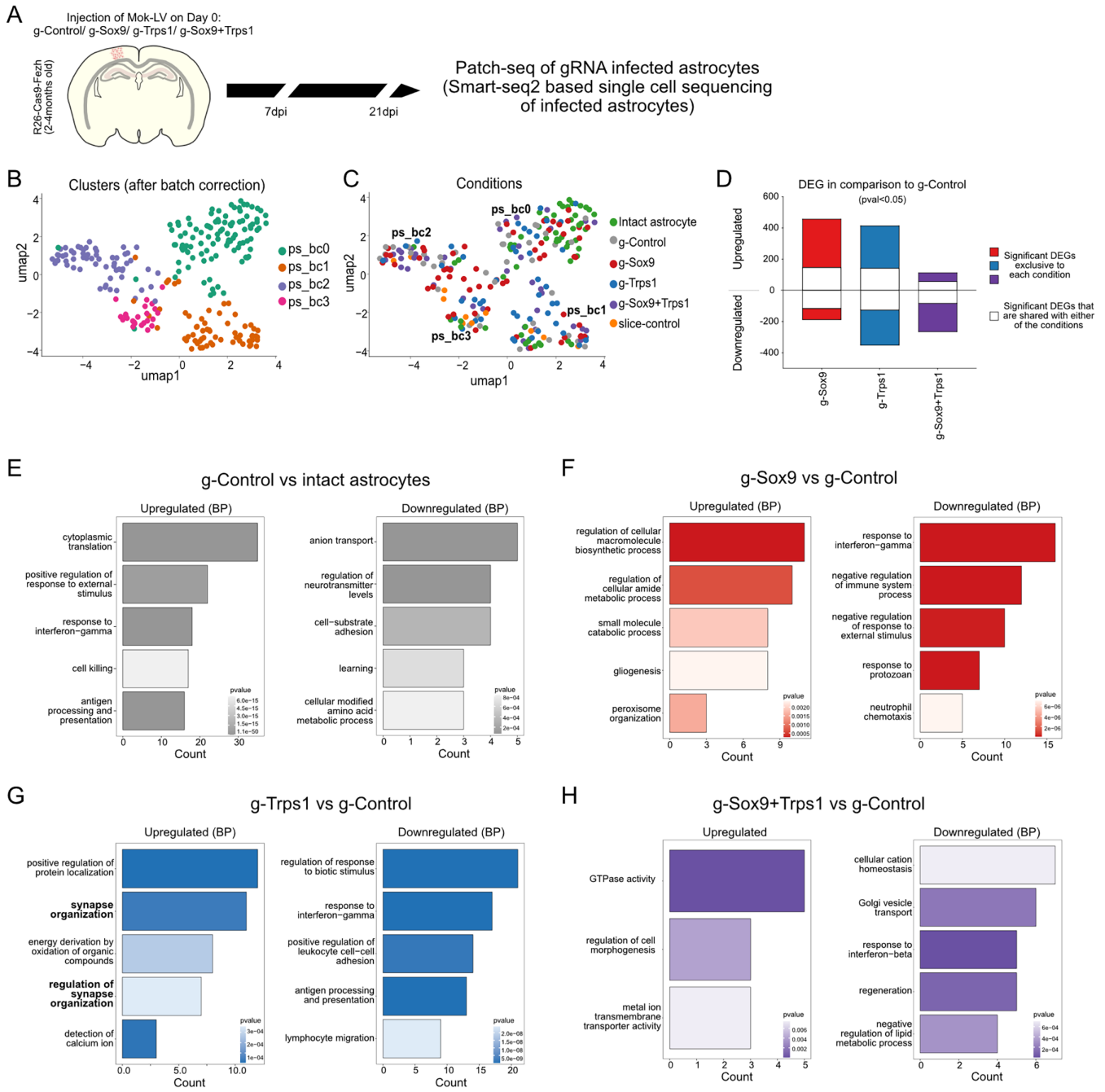
FIGURE 3 | Patch-sequencing of Trps1 and/or Sox9 deleted astrocytes. (A), Scheme for Patch-based scRNA-seq of gRNA infected astrocytes from adult cortex. (B, C) UMAP plots depicting (B) clusters and (C) distribution of experimental conditions across the various clusters. (D) Stacked bar plots showing the number of significantly up and downregulated genes ($p < 0.05$) in g-Sox9, g-Trps1, and g-Sox9+ Trps1 condition in comparison to g-Control. (E–H) Barplots depicting top 5 up- and downregulated pathways enriched in (E) g-Control astrocytes compared to intact astrocytes; in astrocytes after (F) Sox9 deletion, (G) Trps1 deletion, (H) Sox9+ Trps1 deletion in comparison to g-Control. The number of genes enriched in each pathway is shown as "Count"; enrichGO was performed on genes enriched in each condition with p-value < 0.05, and further simplified with Rrvgo package (see Table S3 for more details).

(Figure S5A). Cluster ps_bc2 appears to comprise almost only cells with gRNA injection (irrespective of whether the cells were from control or deletion conditions), suggesting that the cells within cluster ps_bc2 may share a signature related to a response to the mild injury of the Mok-LV injection. Consistently, GO analysis on significantly upregulated genes in g-Control cells compared to intact astrocytes revealed the upregulation of terms like "positive regulation of response to external stimulus," "response

to interferon- gamma," "antigen processing and presentation" (Figure 3E). This indicated an injury response signature that arises because of a mild injury during Mok-LV gRNA injection, also reflecting the reaction to injection of viral vectors (see also Mattugini et al. 2019, for reaction to different viral vectors).

To get a global overview of the effects of Sox9/Trps1 deletion, we performed a pairwise comparison of the deletion conditions
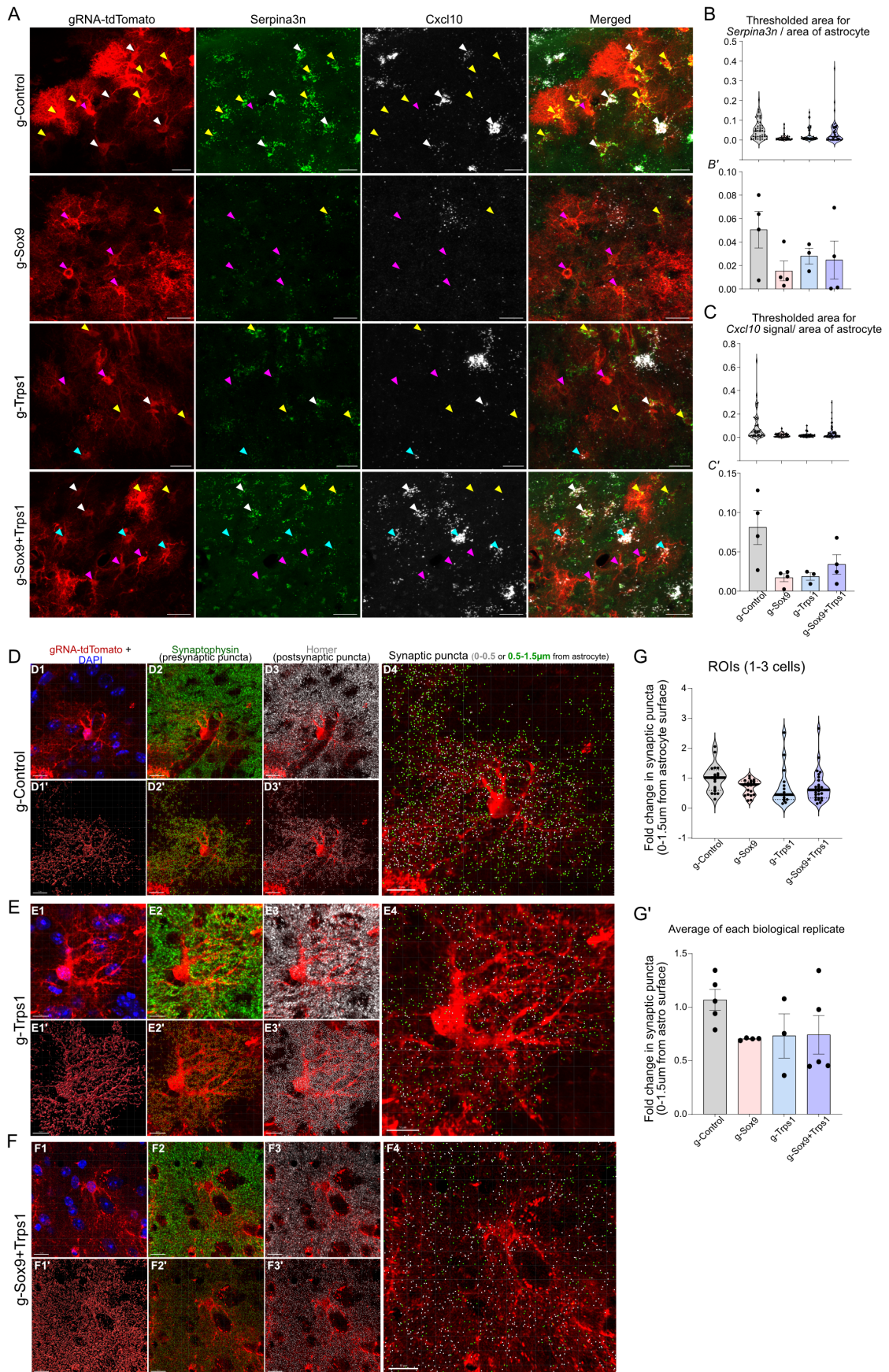
FIGURE 4 | Legend on next page.

with the g-Control cells to understand the gene expression changes irrespective of the time point. Indeed, the deletion of each TF elicited profound changes in gene expression unique to each condition (Figure 3D). Upon Sox9 deletion, 646 significant differentially expressed genes (DEGs) were detected (457 upregulated, 189 downregulated). While most of the upregulated genes were exclusive to the Sox9 deletion condition (Figures 3D, S3D,E), most g-Sox9 downregulated genes were also downregulated after Trps1 or Sox9+ Trps1 deletion (Figure S3F), suggesting a common signature following the deletion of either of these TFs. Trps1 deletion resulted in 767 significant DEGs (414 up-, 353 downregulated), many of which were significant only in the g-Trps1 condition. Following g-Sox9+ Trps1 deletion, fewer significant DEGs were detected, most of which were downregulated (70%, 266 genes) only in this condition (Figures 3D, S3F). These data suggest that Sox9 could be involved in the upregulation of the DEGs after Trps1 deletion and, hence, these up-regulated genes are no longer significant in the double deletion. Vice versa, Trps1 may help upregulating, directly or indirectly, the DEGs that were up-regulated upon the Sox9 deletion, as these upregulated DEGs were strongly reduced in the double-deletion (Figure 3D). However, it is important to bear in mind that protein loss was much less clear in the double deletion, prompting caution in the interpretation of these data.

While Sox9 is known as an activator of transcription (Kang et al. 2012; Ohba et al. 2015), it can also repress genes by competing for co-factors (Yang et al. 2023). Similarly, Trps1 was initially identified as a transcriptional repressor (Fantauzzo et al. 2012; Malik 2001), but could also induce transcription (Fantauzzo and Christiano 2012; Witwicki et al. 2018; Wuelling et al. 2020). Thus, both Sox9 and Trps1 may function as either an activator or a repressor depending on the context. In addition, by 7 and 21 days after gRNA delivery, there is ample time for indirect functions.

3.4 | Considering TF Heterogeneity Across Control Cells for Comparison With TF-Deleted Cells

To determine if the heterogeneous expression of Sox9 and Trps1 could affect the transcriptome analysis, we compared the transcriptome of cells after evaluating the presence of *Sox9* or *Trps1* transcripts. To this end, we first systematically analyzed the reads mapped to the *Sox9* locus in g-Sox9, g-Sox9+ Trps1 and in g-Control and intact astrocytes. We were able to systematically categorize the cells from our scRNA-seq as Sox9 positive (classified as "OK") or Sox9 negative, either because Sox9 was not detected (ND) or had a knockout (KO) due to exon 1 and 2 loss, which were targeted by the Sox9-specific gRNA sequences used. Sox9 transcript could be detected in many control cells; likewise, a clear loss of exon1 and exon2 could be found in most g-Sox9 astrocytes (Figure S5B,D). Sox9+ or Sox9− cells were distributed over identified clusters, though more Sox9+ cells were found in ps_bc0 and Sox9− in ps_bc2 and ps_bc3 (Figure S5C). *Sox9* could be detected in half of intact Aldh1l1-eGFP+ astrocytes and g-Control cells; conversely, only in 25% of g-Sox9 and g-Sox9+ Trps1 astrocytes had reads mapping all *Sox9* exons. (Figure S5D). On the other hand, *Trps1* was not detected in most cells, including the intact and g-Control conditions (Figure S5B,E). Therefore, we compared Sox9-KO cells from g-Sox9 or g-Sox9+ Trps1 conditions and the Sox9+ cells from g-Control astrocytes. Interestingly, most genes were downregulated in the Sox9- cells: 89% of the DEGs (770 genes) in g-Sox9 (Sox9 KO), and 93.6% of the DEGs (1188 genes) in g-Sox9+Trps1 (Sox9 KO) cells (Figure S5F,G). Gene set enrichment analysis (GSEA) revealed changes in pathways like "negative regulation of cell communication," "chromosome organization" in the g-Sox9 condition (Figure S5H) or changes in pathways like "regulation of cellular catabolic process," "carbohydrate derivative biosynthetic process" in the g-Sox9+ Trps1 condition (Figure S5I). However, as we could detect *Sox9* only in a fraction of sequenced cells, while immunofluorescent analysis revealed a reduction of Sox9 in most of the targeted cells (Figure 2F), it is likely that other g-Sox9 astrocytes also lost Sox9 expression. Therefore, we decided focus on the analysis comprising all the cells (Figure 3).

3.5 | Comparison of DEGs With Direct Targets of Sox9 and Trps1

To further explore possible direct targets of Sox9 and Trps1, we overlapped the significant DEGs (Figure 3D) with the known targets of Sox9 and Trps1 based on chromatin-immunoprecipitation-sequencing (ChIP-seq) data for Sox9 in chondrocytes (Ohba et al. 2015) and Trps1 in breast cancer cells (Witwicki et al. 2018). Notably, these TFs share a considerable number of target genes

FIGURE 4 | Effect of Sox9 and Trps1 deletion on injury response related gene expression and synapse numbers. (A) Representative images showing the expression of *Serpina3n* and *Cxcl10* detected by RNAscope in the region of Mok-LV injection at 7 dpi. Infected cells are labeled by immunostaining for the fluorescence reporter (tdTomato). White arrowheads indicate gRNA+ cells expressing *Serpina3n* and *Cxcl10*, magenta arrowheads indicate cells express neither at detectable levels, yellow and cyan arrowheads indicate cells that express one of the two at higher levels (*Serpina3n* high and *Cxcl10* high cells respectively). Scale bars = 20 μm. **(B, C)** Violin plots indicating the thresholded area for the signal of (B) *Serpina3n* and (C) *Cxcl10* in individual cells; (B′ and C′) bar plots indicating the average value of each biological replicate (5–10 cells per animal, n biological replicates = 4 for g-Control, g-Sox9, g-Sox9+ Trps1; n biological replicates = 3 for g-Trps1; not significant). (D–F) Representative images showing gRNA-tdTomato infected astrocytes (D1, E1, F1), their reconstruction on Imaris (D1′, E1′, F1′), immunostaining for presynaptic puncta (D2, E2, F2), the spots considered as pre-synaptic puncta (D2′, E2′, F2′), immunostaining for postsynaptic puncta (D3, E3, F3), spots considered as post-synaptic puncta (D3′, E3′, F3′), the spots considered as synaptic puncta (post-synaptic puncta co-localizing with pre-synaptic puncta, in close proximity to gRNA infected astrocytes at a distance of 0–0.5 (in white) or 0.5–1.5 μm (in green) (D4, E4, F4). Scale bars = 10 μm. (G) Violin plots showing the fold change in the number of synaptic puncta in comparison to g-Control condition; each dot represents a ROI, with 1–3 infected astrocytes in the frame (5–7 ROIs per biological replicate). (G′) Bar plots indicating the average value of each biological replicate (n biological replicates = 4 for g-Control, g-Sox9, g-Sox9+ Trps1; n biological replicates = 3 for g-Trps1; not significant).

(3293 genes, i.e., 53% of Trps1 targets were shared with 33.3% of Sox9 targets, Figure S3G). For the DEGs between Sox9+ and g-Sox9 KO cells (see above), we found 50% to be predicted Sox9 targets (Figure S5J). Likewise, among all g-Sox9 or g-Trps1 versus g-Control cells more than 50% of the DEGs were predicted to be either exclusive Sox9 targets (e.g., *Gbp3*, *Gbp5*, *Ifi35*) or common predicted targets of Sox9 and Trps1 (e.g., *Cdk14*, *Nfix*, *Cpe*) in each condition (Figure S3H, see Table S2 for the entire list of predicted targets), further corroborating the choice to analyze all targeted cells. Interestingly, Sox9 and Trps1 not only share Nfix, another pan-astrocyte TF (Lozzi et al. 2020), as a target, but both also regulate it, suggesting that Sox9, Trps1, and Nfi TFs act in a transcriptional network. Conversely, very few DEGs were predicted to be exclusively targets of Trps1 (around 10%, e.g., *Lamb2*, *Pygl*, *Tmem128*), suggesting that more genes may be regulated by Sox9 or co-regulated by Sox9 and Trps1 in astrocytes. This was likewise the case when we restricted the analysis to the 7dpi time point to avoid even more indirectly regulated genes (50% of the DEGs were predicted targets of Sox9). Thus, even considering all control cells, some of which already have low levels of Sox9 or Trps1, our differential gene expression analysis identified a high proportion of direct target genes, providing confidence in this analysis.

3.6 | Synapse- and Immune-Related Gene Expression Changes Upon Sox9 and/or Trps1 Deletion

To gain more function-oriented insights into the consequences of deleting these TFs, we performed gene ontology (GO) analysis on significant DEGs (log2fold > 0.5; *p*-value < 0.05) in each condition. Interestingly, the analysis of downregulated genes revealed an enrichment of genes associated to immune response, such as "response to interferon-gamma," "response to interferon-beta" but also "regeneration" (i.e., *Igtp*, *Gbp3*; Figure 3F–H; Table S3) in all three deletion conditions (g-Sox9, g-Trps1 and g-Sox9+ Trps1). This may imply an attenuated injury response upon Sox9 and/or Trps1 deletion.

The analysis of genes that were significantly upregulated following TF deletion unraveled common and TF-specific pathways. For instance, synapse-related GO terms were significant in g-Sox9 and g-Trps1 KO conditions ("synapse organization," "neurotransmitter transport," or "secretion"), albeit with different enriched genes (Figure 3F,G; Table S3), thus suggesting altered synapse functions in these conditions. Moreover, genes associated to "gliogenesis" and "glial cell differentiation" pathways were also upregulated (e.g., *Fgfr3*, *Hes5*, *Nfix*, *Zfp365* or *Zfp365*, *Hes1* for g-Sox9 and g-Trps1 respectively; Figure 3F and Table S3). This suggests a possible partial dedifferentiation of the astrocytes upon deletion of Sox9 or Trps1, as many of these genes are active in development or during astrocyte maturation. Remarkably, many genes related to metabolic functions were specifically upregulated in g-Sox9 astrocytes (Figure 3F). The simultaneous deletion of Sox9+ Trps1 upregulated genes related to GTPase activity and morphogenesis (e.g., *Rab6b*, *Rhobtb2*, *Plxnb1*, *Slc23a2*; Figure 3H and Table S3), but not previously mentioned pathways, further suggesting an antagonistic effect of Sox9 and Trps1. Overall, both TFs seem to regulate aspects of synaptic functions, signaling, and gliogenesis.

To better understand the dynamics of gene regulation, we then focused on the early time point (7 dpi) separating the datasets for 7dpi and 21dpi, previously analyzed together. At both time points, fewer DEGs were observed in the g-Sox9+ Trps1 condition, probably due to the above-described cross-regulation and the lower efficiency in protein loss. GO analysis of the DEGs specific to each condition and time point showed consistent downregulation of immune response related pathways ("response to interferon-gamma," "response to interferon-beta," "antigen processing and presentation"; Figure S4A–F). Interestingly, pathways related to "translation" and "signal transduction by p53 class mediator" were only transiently regulated in both g-Sox9 and g-Trps1 conditions at 7 dpi (see Table S4). Taken together, Sox9 and Trps1 appear to converge on common hallmarks of astrocyte function, such as synapse and immune regulation, as well as sharing many direct targets of gene regulation.

3.7 | Loss of Trps1 or Sox9 Triggers Alterations in Inflammatory Response and the Synapses

Having identified both synapse and immune regulation as affected pathways upon Sox9 and Trps1 deletion in astrocytes, we decided to investigate genes involved in these processes. First, we performed RNAscope for *Serpina3n* and *Cxcl10*, two genes associated to immune reaction and specifically upregulated by glial cells in response to injury (Koupourtidou et al. 2024). Interestingly, in all conditions the expression of these injury specific genes in astrocytes was heterogenous (Figure 4A), with some cells expressing both (white arrowheads), none (magenta arrowheads) or one of the two at higher levels (*Serpina3n* high- and *Cxcl10* high-expressing cells; yellow and cyan arrowheads, respectively). In agreement with the significant DEG analysis, a lower level of *Serpina3n* and *Cxcl10* was detected in the targeted astrocytes in all conditions, despite a considerable variation between animals probably due to the strength of the injury elicited by the injection (Figures 4B,C, S6A,B).

Next, we used immunostainings for Vimentin, which is highly expressed in reactive astrocytes, G′ but found downregulated after Sox9 deletion in our dataset, and C1qa, which should be upregulated at the site of injection (Figure S6C). The fluorescence intensity of Vimentin staining showed a trend toward decreased levels in g-Sox9 astrocytes (Figure S6D). Conversely, C1qa immunostaining intensity was higher (as seen by the mean gray value) in gRNA-injected regions in comparison to the corresponding contralateral sides (Figure S6E), indicating an injury-like response. However, we observed no differences between the gRNA conditions.

To explore the effect of Sox9 and Trps1 deletion on synapses, as suggested by GO analysis (Figure 3G for Trps1; Table S3 for Sox9), we immunostained brain sections from different experimental conditions for the pre-synaptic protein synaptophysin and post-synaptic protein Homer1 at excitatory synapses (Figure 4D–F). Interestingly, in g-Trps1 and g-Sox9+Trps1 injected brains, we found a trend toward the reduction in the number of synapses (defined as closely associated pre- and post-synaptic labeling) within 1.5 μm distance around

astrocytes, when compared to the control (Figure 4G, G'), but not when considering only presynaptic or postsynaptic spots independent of their close apposition (Figure S6G,H). This highlights the importance to align pre- and postsynaptic labeling for synapse analysis. A similar trend was observed upon deletion of Sox9 (Figure 4G, G', Figure S6F). Considering that
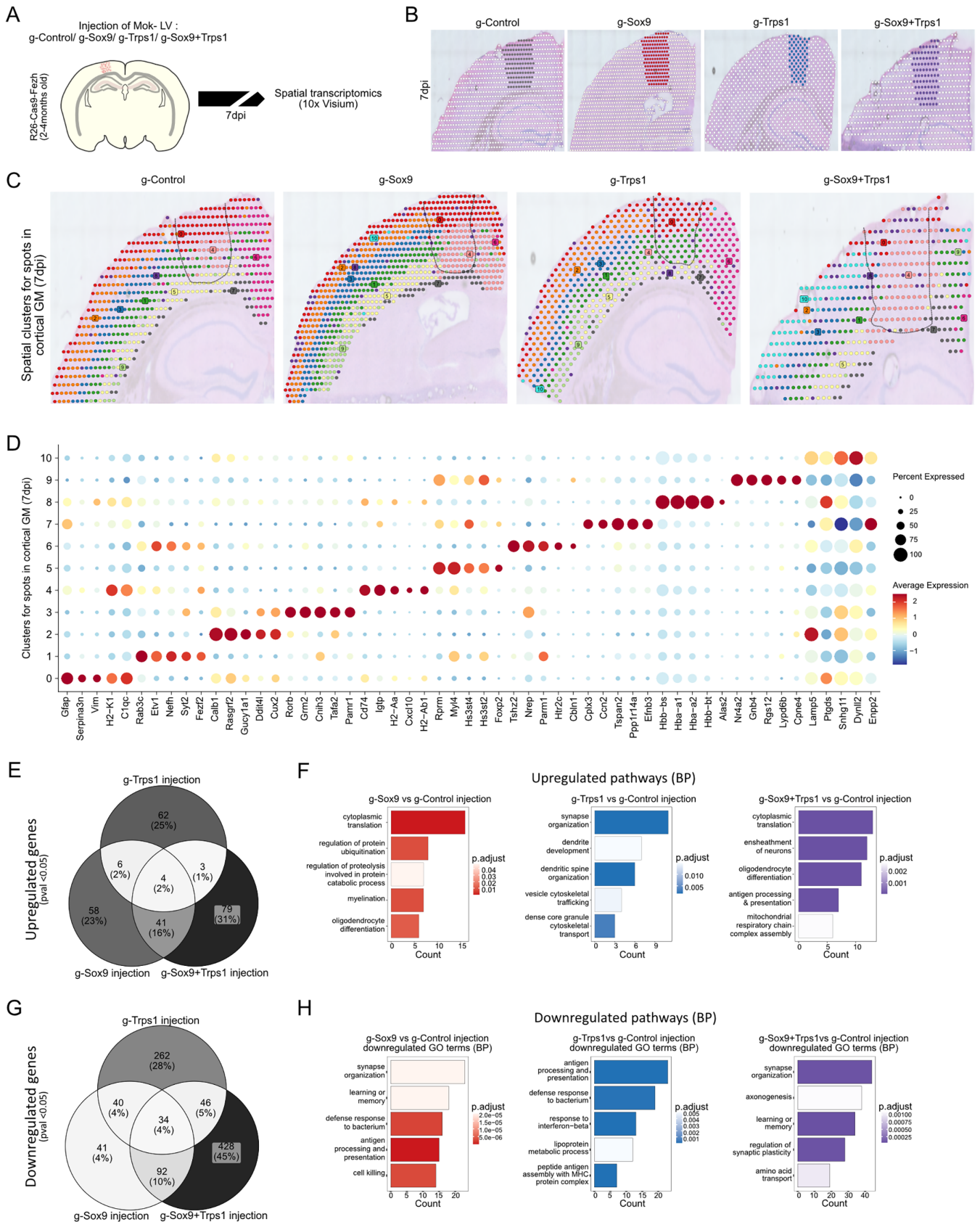

FIGURE 5 | Legend on next page.

this light-microscopic analysis counted many synapses that are not in putative contact with the targeted astrocytes, these data point a possible role of Trps1 and Sox9 in astrocytes for synapse maintenance.

To assess whether the endogenous expression level of Sox9 in the adult intact cortex correlate with the number of synapses in the regions surrounding the astrocytes, we analyzed the number of pre-, post-, and synaptic puncta in close proximity to astrocyte surface, reconstructed based on GFP from Aldh1l1-eGFP mice (Figure S6I,J). Although Sox9 intensity was heterogenous, we could see no correlation between its protein levels, detected by immunostaining, and the number of pre-, post-, or synaptic puncta (Figure S6K–M), suggesting that Sox9 level is not the sole predictor of synapse numbers.

3.8 | Non-Cell Autonomous Effects of Sox9 and Trps1 Deletion in Cortical Astrocytes Revealed by Spatial Transcriptomics

The transcriptomic analysis suggested several functions of Sox9 and/or Trps1 in astrocytes that could impact other cell types, such as neurons and oligodendrocytes (GO analysis in Figure 3, Table S3). To gain better and unbiased genome-wide insights into how alterations of astrocytes lacking Sox9 and/or Trps1 may affect the surrounding cells and tissue microenvironment, we performed spatial transcriptomics (10xGenomics Visium, stRNA-seq) of the adult mouse cortex after injection of g-Control, g-Sox9, g-Trps1 or g-Sox9+Trps1 Mok-LVs. We chose the 7dpi time point to analyze astrocyte response to the injury and their reaction to the Mok-LV injection.

Brains of the animals injected with the Mok-LVs were dissected at 7dpi and 10 μm thick sections prepared at the cryostat. The sections were briefly checked for the presence of infected cells (tdTomato+ cells) in the expected injected region (somatosensory cortex). Once in the region of injection, two consecutive sections containing infected cells were placed in one capture area. The region of injection for each condition was defined based on the fluorescence images taken before tissue processing (Figure 5B). These are referred to as g-Control, g-Sox9, g-Trps1 or g-Sox9+Trps1 injection and the remaining regions are defined as the background regions for the respective experimental conditions henceforth. After quality control steps to remove spots with low gene numbers, counts of high mitochondrial or hemoglobin reads (Figure S7A,B), we clustered the filtered dataset to the cortex GM. This resulted in 11 clusters, which were present in distinct anatomical regions, such

as the different cortex layers (Figure 5C, Figure S7C). These spatial clusters were rather unique in terms of their gene expression signature (Figure 5D). Of particular interest were clusters 0 and 4, which dominated the Mok-LV injection region, but the representation of these clusters was dependent on the condition in consideration (Figure S7D). The spots from the g-Control and g-Sox9 injection were represented in clusters 0 and 4 at comparable levels. On the other hand, cluster 4 dominated the region of g-Sox9+Trps1 injection with very few spots of cluster 0 in this condition. In the g-Trps1 injection, cluster 4 was completely absent, and most spots were represented by cluster 0. Thus, deleting Sox9 or Trps1 in astrocytes resulted in gene expression differences at tissue level. Furthermore, cluster 8 had features associated to injury and Sox9/Trps1 deletion, although it was more sparsely located and was characterized by very few specific genes (Figure S7D,E).

GO analysis on DEGs in clusters 0 and 4 showed the enrichment of genes associated to terms such as "antigen processing and presentation of peptide antigen" "synapse organization," "ion transport" and "microglial cell activation." Furthermore, the GO term "response to interferon-gamma" was significantly specific to clusters 4 and 8, which dominated the g-Sox9+Trps1 tissue: likewise, genes involved in metabolism such as "cellular respiration," "mitochondrial metabolism" were specifically upregulated only in the cluster 0, found in g-Trps1 deletion, (Figure S7F and Table S5). Overall, spatial transcriptomics independently supports the results of our Patch-seq analysis (Figure 3), in particular that Sox9 and/or Trps1 deletion in astrocytes affect the entire reaction of the cortical tissue to injury and g-Trps1 deletion alone affected metabolic pathways (Figure S4C).

Notably, the genetic ablation of Sox9 and Trps1 did not alter the cortical layering: in fact, clusters 7, 5, 9, and 1 represented the deep layers (DL), while clusters 2 and 3 represented the upper layers (UL, Figure 5C), as confirmed by the expression pattern of known or predicted UL and DL neuronal and astrocyte markers (Figure S7G). A prominent exception to this was in the tissue of g-Sox9+Trps1, where the cluster 10 replaced the UL cluster 2. Even though cluster 10 is in the same anatomical position as cluster 2, it showed a unique gene expression signature, with only 8% of the genes being common with cluster 2 (Figure S7H). GO analysis of genes unique to this cluster showed the enrichment of pathways, such as "cytoplasmic translation," "antigen processing and presentation," "exocytosis" (Figure S7I and Table S5), pointing to possible widespread tissue level effects unique to the simultaneous deletion of Sox9 and Trps1 in astrocytes.

FIGURE 5 | Tissue level effects of Sox9 and Trps1 deletion in cortical astrocytes explored by Spatial transcriptomics. (A) Scheme for Spatial transcriptomics (10xGenomics Visium, stRNA-seq) in the cortex of adult mice injected with Mok-LV expressing gRNA. Cortices injected with either g-Control, g-Sox9, g-Trps1 or g-Sox9+Trps1 were manually resected and two consecutive sections with infected cells were placed in one capture area each of a 10xGenomics Visium slide. (B) Spatial location of the gRNA injection region (defined based on the fluorescence signal in the images taken before tissue processing steps) is highlighted for each condition; the remaining tissue is considered as background tissue for each condition. (C) Spatial distribution of clusters for spots specific to cortical GM across all conditions, region of injection demarcated with a dotted line in each sample. (D) Dot plot showing expression of top 5 genes for each of the spatial clusters. (E–H) Pie charts depicting overlap of (E) up- and (G) downregulated genes in the injection regions after Sox9/Trps1 deletion in comparison to Control injection. Bar plots depicting top 5 (F) upregulated and (H) downregulated pathways enriched in the injection regions after Sox9/Trps1 deletion in comparison to Control injection. The number of genes enriched in each pathway is shown as "Count"; enrichGO was performed on genes enriched in each condition with $p < 0.05$ and further simplified with Rrvgo package. See Table S5 for more details.

To get an overview of the transcriptomic differences in the areas after the deletion of the TFs, we compared g-Sox9, g-Trps1, and g-Sox9+Trps1 injected regions with their g-Control counterpart (injected regions defined by fluorescent labeling). Overall, we detected more downregulated than upregulated genes in any pair-wise comparison (Figure 5E,G). Most of upregulated

DEGs were specific to one condition, with only very few genes significantly upregulated in all three conditions (Figure 5E). Likewise, only 4% of the downregulated genes were common to all the conditions (Figure 5G). Intriguingly, the g-Sox9+Trps1 condition showed the highest number of downregulated genes, followed by Trps1 deletion. Most of such downregulated genes
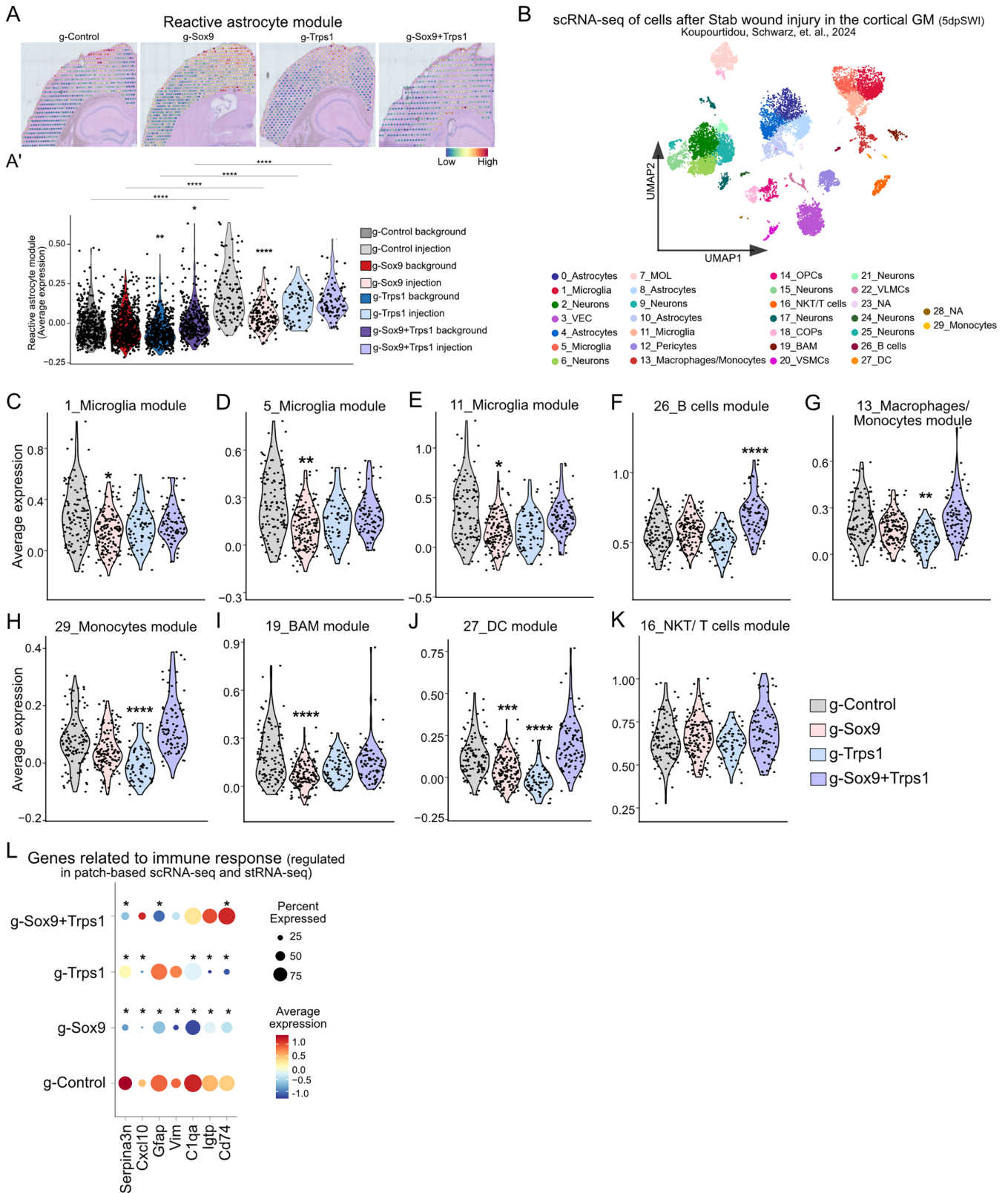
FIGURE 6 | Legend on next page.

were distinct and not overlapping with the other conditions (Figure 5G). Conversely, most of the downregulated genes in g-Sox9 injected area were common to other conditions (Figure 5G), thus suggesting that Sox9 deletion might trigger a more generic tissue response.

Gene ontology analysis on the DEGs between the regions of injection targeted by the different gRNAs provided interesting insights: for instance, genes upregulated in the g-Sox9 and g-Sox9+Trps1 injection were associated to "oligodendrocyte differentiation" (e.g., *Olig1*, *Enpp2*, *Tspan2*, etc.) (Figure 5F). This suggests that the deletion of Sox9/Trps1 in astrocytes may affect oligodendrocyte function or differentiation (see below). On the other hand, genes related to "antigen processing and presentation" were downregulated in g-Sox9 and g-Trps1 injection (Figure 5H), revealing a dampened immune response after the loss of Sox9, Trps1. Overall, stRNA-seq independently supported the involvement of Sox9 and Trps1 in regulating astrocyte functions at the synapse and in immune reaction to the mild injury.

3.9 | Crosstalk Between Astrocytes and Other Cell Types After Sox9 and Trps1 Deletion

To gain a deeper insight on how genetic manipulation of astrocytes affect other cell types, we employed gene module scores (Hasel et al. 2021; Sadick et al. 2022). For example, the spots in the UL and DL showed a higher score for the corresponding modules of UL and DL neuronal markers (Figure S8A).

First, we computed the module score for genes known to be specifically upregulated in reactive astrocytes (Table S7). As expected, this score was significantly higher in all injected regions in comparison to their corresponding background tissue (Figure 6A,A′; Table S7 for the summary of injection-specific changes; background is considered as the region outside the fluorescently labeled injection areas). Among the injected regions, only the score of g-Sox9 area was significantly lower than the g-Control injection.

The level of Gfap in astrocytes is a good measure of general tissue pathology (Escartin et al. 2021; Hol and Pekny 2015). Therefore, its protein level was examined by fluorescence intensity measurement after immunostaining. Notably, the mean intensity of Gfap-immunosignal increased threefold in the g-Trps1 conditions at 7dpi (Figure S8B). As the expression dynamics could

differ between RNA and protein, we performed the same analysis at 21 dpi and found that cells from the g-Sox9 and g-Trps1 showed a reduced Gfap intensity to half compared to g-Control (Figure S8C). Overall, these data further supported a reduced astrocyte reactivity upon Sox9 or Trps1 deletion in the region after Sox9 and Trps1 deletion.

3.10 | Comparison to scRNAseq Data of Reactive Glia After Brain Injury

To better link the changes in the stRNA-seq data to individual reactive glial cell types, we took advantage of recently published sc- and stRNA-seq dataset on stab wound-injured adult mouse forebrain (Koupourtidou et al. 2024). Among the data, we considered 5 days post stab wound (5dpSWI) as dataset to compare, as it is closer to our time point of 7dpi. In addition to several clusters of neurons, astrocytes, microglia, and oligodendrocytes, other cell types were present in the dataset, including B cells, NKT (natural killer T (NKT)/T cells) cells, border-associated macrophages (BAM), dendritic cells (DC), vascular endothelial cells (venous) (VECV), vascular smooth muscle cells (VSMCs) (Figure 6B). This study also identified the presence of an injury-specific spatial cluster using the same stRNA-seq analysis. We first computed the module score for the top 50 genes of their injury-specific cluster to verify that the published experimental paradigm was comparable to ours. Indeed, we found that the expression of these injury-specific genes was significantly higher in all the injected regions in comparison to the corresponding background regions (Figure S8D,E), thus supporting the use of the SWI data to leverage our experimental paradigm of Mok-LV injection.

3.10.1 | Reactive Astrocyte Analysis

To understand if the deletion of Sox9, Trps1, or both lead to the presence of cell types different from those found in 5dpSWI scRNA-seq data, we computed module scores based on the top DEGs for each of these annotated cell type clusters by Koupourtidou et al. (2024). While the module score for reactive astrocyte genes was significantly upregulated in all the injection regions (Figure 6A,A′), the module scores for the various astrocyte clusters were largely unaltered (Figure S8F–I). Only the g-Sox9 injected region showed a significant downregulation in two astrocyte clusters (4_Astrocytes and 10_Astrocytes), while g-Trps1 injected region scored slightly

FIGURE 6 | Altered immune response after Sox9, Trps1 deletion. (A) The extent of "Reactive astrocyte module" gene expression in different conditions shown in (A) Spatial Feature plots and (A′) Violin plots (stratified based on region of gRNA injection and corresponding background tissue) respectively. (B) UMAP plot depicting distribution of cells collected 5 days post stab wound injury (dpSWI) in the cortex GM, clusters are color-coded according to the cell type annotation (Koupourtidou et al. 2024). (C–K) Violin plots depicting module scores for (C) 1_Microglia, (D) 5_Microglia, (E) 11_Microglia, (F) 26_B cells, (G) 13_Macrophages/Monocytes, (H) 29_Monocytes, (I) 19_BAM, (J) 27_DC, (K) 16_NKT/T cells. Module scores computed based on the top 25 DEG for each of the annotated cell type clusters present in the 5dpSWI scRNA-seq of Koupourtidou et al. (2024). Statistics for comparing module scores A′, (C–K) done using Kruskal-Wallis test and Dunn's multiple comparison. Significance for comparisons (in A′) of the injection regions with the corresponding background tissue depicted with lines and * above; significance for comparisons of experimental injection regions with the control-injection (A′, C–K) depicted with * above the respective violins; *p ≤ 0.05, **p ≤ 0.005, ***p ≤ 0.0005, ****p ≤ 0.0001. Refer to Table S7 for the list of genes used for module score calculation and a summary of the changes in different conditions. BAM = border-associated macrophages, DC = dendritic cells; dpSWI = days post stab wound injury, NKT = natural killer T cells. (L) Dot plots showing the expression of genes in the stRNA-seq data contributing to injury response (also differentially expressed in patch-based scRNA-seq), significant DEGs in comparison to g-Control injection are denoted by "*" above the corresponding dots.

higher in one of the astrocyte clusters (8_Astrocytes). In summary, this analysis indicated an ongoing overall reactive state of astrocytes which cannot be attributed to a specific astrocyte subcluster.

3.10.2 | Microglia and Immune Cell Analysis

Next, we computed module scores for microglia and other immune cell types to understand the effects of astrocyte manipulation on these cell types. All injected regions showed a significantly elevated microglia module score (for all three microglia substrates), as well as increased module scores for other immune cells such as B cells, monocytes, macrophages, T cells, BAM and DC in comparison to the corresponding background regions, indicating that this is an injury specific response (see Table S7.2 for summary). Notably, the score of the g-Sox9 condition was significantly lower than the g-Control injection in all the microglia cluster modules (Figure 6C–E, Table S7.1), but not the g-Sox9+Trps1 injected region. Thus, the reduced immune response in astrocytes upon Sox9 deletion (Figure 3E–G) may also be due to reduced microglial activation.

Among the other immune cells that respond to injury, we found an increase in B cell representation in g-Sox9+Trps1 injection, as highlighted by high B cell module (Figure 6F, Table S7.1). Only the g-Trps1 injected region showed attenuated score for monocytes module (Figure 6G,H) and only g-Sox9 injected region showed attenuated score for the BAM module (Figure 6I), while both g-Sox9 and g-Trps1 injected regions showed a significant reduction in DC module in comparison to the g-Control injection (Figure 6J). The module score of NKT/T cells (Figure 6K) was not significantly altered in any of the experimental conditions. Furthermore, many genes related to immune response that were significantly downregulated in the Patch-seq analysis were also downregulated in the stRNA-seq data (Figure 6L).

In summary, Sox9 and Trps1 seem to contribute to regulate communication with various immune cells after the injury caused by viral vector injection, which is reduced upon deleting these TFs.

3.10.3 | Oligodendrocyte Cell Analysis

Module scores for the various oligodendrocyte lineage clusters recapitulated the effects observed earlier in the GO term analysis, namely the increased oligodendrocyte differentiation (Figure 5F). Only the g-Trps1 injected region showed a slightly elevated score for the OPCs module (oligodendrocyte precursor cells, Figure S8J). Interestingly, both g-Sox9 and g-Sox9+Trps1 scored significantly higher in the modules for committed oligodendrocyte progenitors (COPs, Figure S8K) and mature oligodendrocytes (MOL, Figure S8L).

Taken together, these data demonstrate changes in immune cell responses at tissue level, depending on the manipulated TFs and possible effects on oligodendrocyte differentiation as well. To explore if there is an increased proliferation or

presence of newly differentiated oligodendrocytes, we performed Sox9, Trps1 deletion along with BrdU incorporation (Figure S9). Indeed, the number of Bcas1+ cells (recently differentiated oligodendrocytes) as well as the number of BrdU+/Bcas1+ cells are doubled in the g-Trps1 condition (Figure S9D–G). Conversely, no obvious trend toward any changes was observed for the number of Olig2+ cells (oligodendrocyte progenitor population) incorporating BrdU (Figure S9H–K).

Both Patch-seq and stRNA-seq analysis show that the astrocyte-specific deletion of Sox9 and/or Trps1 triggers a multitude of non-cell autonomous effects, shaping the injury response by attenuating astrocyte, microglia and immune cell reactions in various combinations, and affecting oligodendrocyte differentiation, which may be beneficial for repair.

4 | Discussion

Here, for the first time, we elucidated the functions of the novel astrocyte TF Trps1 in the brain. Using astrocyte-specific deletion followed by single-cell and tissue-wide transcriptomic analysis, we showed that Trps1 in astrocytes affects synapse maintenance as well as astrocyte reaction to a mild injury. Interestingly, Trps1 deletion in astrocytes also acts in a non-cell-autonomous manner, as it affects oligodendrocytes and specific immune cells, such as monocytes. Deletion of the pan-astrocyte TF Sox9 in astrocytes revealed similar roles in regulating genes involved in synapse function and the immune reaction of astrocytes, with intriguingly distinct effects on other immune cells. Consistent with these TFs acting in a transcriptional network in other cell types, we found a large overlap of known target genes to be regulated by Trps1 and Sox9 and fewer genes regulated when both factors were deleted, but also surprising effects on immune cells only upon deletion of both TFs. This highlights their potential cross-regulation and functional interaction within the same molecular pathways and, thus, identified a novel transcriptional regulome of specific astrocyte functions in the adult cerebral cortex.

4.1 | Heterogeneous Expression of Trps1 and Sox9 in Cortical GM Astrocytes

Here we show the localization and function of Trps1 as a novel TF in astrocytes. Notably, Trps1 protein was detectable in a subset of astrocytes (40% of S100β+/Sox9+) with a bias to deeper cortex layers. Astrocyte diversity at the level of cortical layers has already been characterized (Bayraktar et al. 2020; Lanjakornsiripan et al. 2018) and is influenced by neurons when establishing the layers. While the layer-specific function of Trps1 in astrocytes is still unknown, its effects on synapse maintenance, as discussed below, may be most prominent in deep layer cortex neurons. Moreover, we also observed Trps1 in about half of Olig2+ cells of the oligodendrocyte lineage in the adult brain, reminiscent of its role as transcriptional regulator of both astrocyte and oligodendrocyte fate in development (Weng et al. 2019). It is also worth noting that Trps1 protein levels are highest in the deep layers with the

highest myelination in the cortex (Palomero-Gallagher and Zilles [2019](#); Rowley et al. [2015](#)). Taken together, Trps1 is expressed in a subset of adult astrocytes, which endows them with specific properties.

In contrast to Trps1, Sox9 was expressed in most but not all astrocytes (between 60% and 90%) throughout the cortex, even though with varying intensities throughout the cortical column (Figure 1C,D,F). Remarkably, the heterogeneity at the protein level is mirrored by heterogeneity at the mRNA level observed among cortex GM astrocytes. Thus, eventhough Sox9 is often considered a "pan-astrocyte" marker, its expression varies across astrocytes, raising the question of whether such heterogeneous expression has any functional relevance.

4.2 | Trps1 and/or Sox9 Deletion Sheds Light on Their Functions in Cortical GM Astrocytes

CRISPR/Cas9-mediated gene deletion is a powerful tool to explore gene function, but its cell-type-specific targeting is essential to explore cell-autonomous effects. Indeed, we demonstrated that Mokola pseudotyping of lentiviral vectors is an efficient way to achieve astrocyte-specific targeting, as most cells infected with the g-Control were immunopositive for the astrocyte markers S100β, Gfap and Sox9 at 7 and 21 dpi (Figure 2D,E). CRISPR/Cas9-mediated deletion of Sox9 and Trps1 was efficient, as most cells no longer expressed the protein targeted by CRISPR deletion and such loss was complete by 7 dpi (Figure 2F,G).

Patch-seq revealed that Trps1 deletion resulted in a comparable number of up- and down-regulated genes, which is consistent with the versatile role of Trps1 both as a transcriptional repressor (Fantauzzo et al. [2012](#); Malik [2001](#)) and activator (Fantauzzo and Christiano [2012](#); Witwicki et al. [2018](#); Wuelling et al. [2020](#)). Conversely, Sox9 deletion resulted in more upregulated genes, which is not consistent with its main role as a transcriptional activator (Kang et al. [2012](#); Ohba et al. [2015](#)). However, our analysis was done 7 days after gRNA injection, thus providing enough time for indirect gene regulation, and Sox9 can act as a repressor as well (Leung et al. [2011](#); Yang et al. [2023](#)). In addition, the overlap of the DEGs with ChIP-seq data of Sox9 and Trps1, albeit from different cell types (Ohba et al. [2015](#); Witwicki et al. [2018](#)), was remarkably large, with more than 50%, thus suggesting that many direct targets are still regulated at 7 dpi (Figure S3H).

Notably, Sox9-Trps1 simultaneous deletion resulted in fewer DEGs, with the least number of upregulated genes, hinting at a possible cross-regulation, such as, for example, Sox9 required to activate the targets de-repressed by Trps1. However, these results may also reflect the less efficient protein loss in this condition. Nevertheless, the deletion of both factors also suggests specific effects on B cells, not apparent in the single deletion at spatial transcriptomic level. In the hair follicle epithelium, Trps1 negatively regulates *Sox9* expression (Fantauzzo et al. [2012](#)), while in chondrocytes, Sox9 induces *Trps1* expression (Tan et al. [2018](#)), highlighting the notion that these TFs cross-regulate each other in different ways in different tissues. Here, we show that the deletion of Sox9 and Trps1 in adult brain astrocytes also exhibit interacting effects and partial overlapping functions, with similar GO terms detected in Sox9 and Trps1 low-expressing astrocytes.

A common effect of deleting either Sox9 or Trps1 was the upregulation of genes related to gliogenesis (i.e., *Fgfr3*, *Hes5*, *Zfp365* or *Hes1*, *Zfp365*; Figure 3F, Table S3). This may serve to stabilize glial identity, thus maintaining astrocyte identity even in the absence of Sox9 or Trps1. Furthermore, the loss of either Sox9 or Trps1 showed effects on synapse-related gene expression (g-Sox9, Table S3; g-Trps1, Figure 3G). This suggests functional alterations at the synapses and/or regulation of synapse numbers, as astrocytes have been implicated in synapse formation, maintenance and even pruning (Allen and Eroglu [2017](#); Chung, Allen, and Eroglu [2015](#); Lee et al. [2021](#)). To examine the synapses, we quantified the number of synaptic puncta in close proximity to the infected astrocytes (Figure 4D–G). This revealed a reduction of synaptic punctae upon Trps1 or Sox9-Trps1 double deletion, albeit not reaching significance between different animals (see limitation of the study below). The role of Sox9 at synapses may affect other aspects, such as shown in previous work in the olfactory bulb, where it regulates astrocyte response to inhibitory neurons during development (Cheng et al. [2023](#)).

Another common effect of Sox9 and Trps1 deletion was the downregulation of immune response-related pathways (Figure 3F–H). Indeed, we could detect a non-significant reduction in the expression of *Serpina3n* and *Cxcl10*, which are typically upregulated in all glial cells under inflammatory conditions (Koupourtidou et al. [2024](#)), following the deletion of Sox9 and Trps1 (Figure 4B,C). Astrocyte-specific *Serpina3n* expression exacerbates neuroinflammation in an epileptic mice model (Liu et al. [2023](#)), and the human orthologue has been implicated in blood brain barrier dysfunction (Kim et al. [2022](#)) and even in Alzheimer's disease progression (Nilsson et al. [2001](#); Padmanabhan et al. [2006](#)). *Cxcl10* has been identified as a gene expressed in a unique subset of astrocytes that upregulate interferon response after inflammation and such astrocytes are also enriched in Alzheimer's disease and multiple sclerosis (Hasel et al. [2021](#); Prakash et al. [2024](#)). Thus, the impact of Sox9 and Trps1 loss on key genes involved in distinct inflammatory reactions underscores a possible contribution to astrocyte-mediated neuroinflammatory processes.

Taken together, single-cell analysis revealed some functions of Trps1 and Sox9 in astrocytes of the cerebral cortex, the later previously missed at the tissue level. This shows that Sox9 and Trps1 play multiple common roles, including those on synaptic contacts and immune response.

4.3 | Astrocyte-Specific Trps1 and/or Sox9 Deletion Triggers Non-cell Autonomous Effects and an Imbalance in Glial and Immune Cell Response

Astrocytes are integral to the tripartite synapse communication and, hence, can act in a cell-autonomous and/or non-cell-autonomous manner at synapses. Additionally, astrocytes signal to many other cell types, especially after injury (Kim et al. [2022](#); Koupourtidou et al. [2024](#)). To explore non-cell-autonomous effects in our mild injury condition, we performed spatial transcriptomic analysis, which revealed novel and widespread tissue level changes upon Sox9 and/or Trps1 deletion in astrocytes. Among the injury-responsive spatial clusters, cluster 0 was

characterized by the higher expression of known reactive glial genes (e.g., *Gfap*, *Serpina3n*, *Vim*), while cluster 4 was characterized by expression of genes such as *Igtp*, *Cxcl10*, which are involved in the interferon response (Figure 5D). Similar to the results of Patch-seq, stRNA-seq indicated dampened immune responses in the tissue region, where Trps1 or Sox9 was deleted. RNAscope shed the downregulation of *Serpina3n* and *Cxcl10* upon either Trps1 or Sox9 deletion (Figure 4A–C), demonstrating reliability of both these datasets.

In contrast, Sox9-Trps1 double deletion showed an increased immune activation in the cortex, a notably different response to the single deletions. It is tempting to speculate that the simultaneous Sox9 and Trps1 deletion (g-Sox9+Trps1 injection) leads to a reduced ability of astrocytes to coordinate the immune response, which either results in or is compensated by the activation of other cells, such as microglia and invading monocytes, thus causing a broader immune response in that region. Indeed, the latter seems to be more plausible, as the comparison of our stRNA-seq data after astrocyte-specific Sox9 and/or Trps1 deletion with the scRNA-seq data of cells from cortical GM after a stab wound injury (Koupourtidou et al. 2024) revealed an increased expression of B cell-specific genes in the tissue after both Sox9 and Trps1 deletion. On the other hand, in g-Sox9 or g-Trps1 single deletion the tissue had significantly reduced expression of genes enriched in microglia, monocytes, T cells or DCs (see Table S7 for summary). Intriguingly, however, there is surprising specificity: Sox9 deletion affects microglia gene expression, while Trps1 deletion affects monocyte gene expression. It will be very interesting to explore the signaling pathways mediating this astrocyte-specific effect on immune cell responses in an injury condition.

A further notable observation is that astrocyte-specific Sox9 or Sox9+Trps1 deletion elicited a prominent increase in representation of oligodendrocytes gene expression (18_COPs and 7_MOL) as well as the upregulation of GO terms such as "oligodendrocyte differentiation." In zebrafish brain injury, increased OPC proliferation and accumulation at the site of injury are regulated by the immune response pathways (Tlr2, Cxcr3) (Sanchez-Gonzalez et al. 2022). Reactive astrocytes may also influence the rate of oligodendrocyte differentiation via endothelin-1/Ednrb signaling (Hammond et al. 2015). Thus, the effects of the manipulation of astrocytes on oligodendrocyte differentiation, as monitored by Bcas1+ cells incorporating BrdU, may be mediated via the immune cells or by direct signaling.

Taken together, our work shows that the manipulation of few astrocytes can have profound effects on other glial and immune cells, highlighting the key role of the novel astrocyte transcription factor Trps1 in this process, as well as revealing a previously unknown role for Sox9, not only in postnatal development or other brain regions (Cheng et al. 2023; Ung et al. 2021), but also in the adult cortex astrocytes. This was unraveled by the mild injury condition elicited by the Mok-LV injection, which challenges the astrocytes such that the consequences of TF deletion are more prominent and sheds light on astrocyte functions that are compromised in the absence of key TFs like Sox9 and Trps1. Likewise, *Rbpj-k* knockdown in cortical astrocytes had an observable effect only when combined with a SWI (Zamboni et al. 2020), and cortical astrocytes may, in general, be more resistant to gene perturbations (at least in the context of genes like *Rbpj-k*, *Sox9*, and *Nfia* that have been studied so far). At the molecular level, we found a surprising overlap in the function and effects elicited by Sox9 and Trps1 deletion, corroborating the functional interactions of these TFs, which have also been observed in other tissues (Shibata et al. 2016; Tan et al. 2018). Taken together, the novel astrocyte TF Trps1 aligns functionally with Sox9 in regulating predominantly synaptic and immune functions in mildly reactive astrocytes.

4.4 | Limitation of the Study

While the mild injury caused by the viral vector injection into the cerebral cortex revealed some phenotypes affected by Trps1 and Sox9 deletion, this is also at the same time the limitation of the study. On one side because it cannot assess the function of these TFs in an entirely intact and homeostatic brain environment; on the other side because it introduces a notable variability between the injections in the different animals. Therefore, many of the strong trends (doubling or triple the number of cells) are not statistically significant across animals.

Conflicts of Interest

The authors declare no conflicts of interest.

Data Availability Statement

Data are available at Gene Omnibus (GEO) ID: GSE279676.

References

Allen, N. J., and C. Eroglu. 2017. "Cell Biology of Astrocyte-Synapse Interactions." *Neuron* 96: 697–708. https://doi.org/10.1016/j.neuron.2017.09.056.

Bayraktar, O. A., T. Bartels, S. Holmqvist, et al. 2020. "Astrocyte Layers in the Mammalian Cerebral Cortex Revealed by a Single-Cell In Situ Transcriptomic Map." *Nature Neuroscience* 23: 500–509. https://doi.org/10.1038/s41593-020-0602-1.

Breunig, C. T., A. M. Neuner, J. Giehrl-Schwab, W. Wurst, M. Götz, and S. H. Stricker. 2018. "A Customizable Protocol for String Assembly gRNA Cloning (STAgR)." *Journal of Visualized Experiments* 142: 58556. https://doi.org/10.3791/58556.

Cadwell, C. R., A. Palasantza, X. Jiang, et al. 2016. "Electrophysiological, Transcriptomic and Morphologic Profiling of Single Neurons Using Patch-Seq." *Nature Biotechnology* 34: 199–203. https://doi.org/10.1038/nbt.3445.

Cadwell, C. R., F. Scala, S. Li, et al. 2017. "Multimodal Profiling of Single-Cell Morphology, Electrophysiology, and Gene Expression Using Patch-Seq." *Nature Protocols* 12: 2531–2553. https://doi.org/10.1038/nprot.2017.120.

Cheng, Y.-T., E. Luna-Figueroa, J. Woo, et al. 2023. "Inhibitory Input Directs Astrocyte Morphogenesis Through Glial GABABR." *Nature* 617: 369–376. https://doi.org/10.1038/s41586-023-06010-x.

Chung, W.-S., N. J. Allen, and C. Eroglu. 2015. "Astrocytes Control Synapse Formation, Function, and Elimination." *Cold Spring Harbor Perspectives in Biology* 7: a020370. https://doi.org/10.1101/cshperspect.a020370.

Deneen, B., R. Ho, A. Lukaszewicz, C. J. Hochstim, R. M. Gronostajski, and D. J. Anderson. 2006. "The Transcription Factor NFIA Controls the Onset of Gliogenesis in the Developing Spinal Cord." *Neuron* 52: 953–968. https://doi.org/10.1016/j.neuron.2006.11.019.

Endo, F., A. Kasai, J. S. Soto, et al. 2022. "Molecular Basis of Astrocyte Diversity and Morphology Across the CNS in Health and Disease." *Science* 378: eadc9020. https://doi.org/10.1126/science.adc9020.

Escartin, C., E. Galea, A. Lakatos, et al. 2021. "Reactive Astrocyte Nomenclature, Definitions, and Future Directions." *Nature Neuroscience* 24: 312–325. https://doi.org/10.1038/s41593-020-00783-4.

Fantauzzo, K. A., and A. M. Christiano. 2012. "Trps1 Activates a Network of Secreted Wnt Inhibitors and Transcription Factors Crucial to Vibrissa Follicle Morphogenesis." *Development* 139: 203–214. https://doi.org/10.1242/dev.069971.

Fantauzzo, K. A., M. Kurban, B. Levy, and A. M. Christiano. 2012. "Trps1 and Its Target Gene Sox9 Regulate Epithelial Proliferation in the Developing Hair Follicle and Are Associated With Hypertrichosis." *PLoS Genetics* 8: e1003002. https://doi.org/10.1371/journal.pgen.1003002.

Gibson, D. G. 2011. "Enzymatic Assembly of Overlapping DNA Fragments." In *Methods in Enzymology*, vol. 498, 349–361. Amsterdam: Elsevier. https://doi.org/10.1016/B978-0-12-385120-8.00015-2.

Glasgow, S. M., J. C. Carlson, W. Zhu, et al. 2017. "Glia-Specific Enhancers and Chromatin Structure Regulate NFIA Expression and Glioma Tumorigenesis." *Nature Neuroscience* 20: 1520–1528. https://doi.org/10.1038/nn.4638.

Hammond, T. R., B. McEllin, P. D. Morton, M. Raymond, J. Dupree, and V. Gallo. 2015. "Endothelin-B Receptor Activation in Astrocytes Regulates the Rate of Oligodendrocyte Regeneration During Remyelination." *Cell Reports* 13: 2090–2097. https://doi.org/10.1016/j.celrep.2015.11.002.

Hasel, P., I. V. L. Rose, J. S. Sadick, R. D. Kim, and S. A. Liddelow. 2021. "Neuroinflammatory Astrocyte Subtypes in the Mouse Brain." *Nature Neuroscience* 24: 1475–1487. https://doi.org/10.1038/s41593-021-00905-6.

Heinrich, C., M. Bergami, S. Gascón, et al. 2014. "Sox2-Mediated Conversion of NG2 Glia Into Induced Neurons in the Injured Adult Cerebral Cortex." *Stem Cell Reports* 3: 1000–1014. https://doi.org/10.1016/j.stemcr.2014.10.007.

Hol, E. M., and M. Pekny. 2015. "Glial Fibrillary Acidic Protein (GFAP) and the Astrocyte Intermediate Filament System in Diseases of the Central Nervous System." *Current Opinion in Cell Biology* 32: 121–130. https://doi.org/10.1016/j.ceb.2015.02.004.

Huang, A. Y.-S., J. Woo, D. Sardar, et al. 2020. "Region-Specific Transcriptional Control of Astrocyte Function Oversees Local Circuit Activities." *Neuron* 106: 992–1008.e9. https://doi.org/10.1016/j.neuron.2020.03.025.

Kang, P., H. K. Lee, S. M. Glasgow, et al. 2012. "Sox9 and NFIA Coordinate a Transcriptional Regulatory Cascade During the Initiation of Gliogenesis." *Neuron* 74: 79–94. https://doi.org/10.1016/j.neuron.2012.01.024.

Kim, H., K. Leng, J. Park, et al. 2022. "Reactive Astrocytes Transduce Inflammation in a Blood-Brain Barrier Model Through a TNF-STAT3 Signaling Axis and Secretion of Alpha 1-Antichymotrypsin." *Nature Communications* 13: 6581. https://doi.org/10.1038/s41467-022-34412-4.

Klum, S., C. Zaouter, Z. Alekseenko, et al. 2018. "Sequentially Acting SOX Proteins Orchestrate Astrocyte- and Oligodendrocyte-Specific Gene Expression." *EMBO Reports* 19: e46635. https://doi.org/10.15252/embr.201846635.

Koupourtidou, C., V. Schwarz, H. Aliee, et al. 2024. "Shared Inflammatory Glial Cell Signature After Stab Wound Injury, Revealed by Spatial, Temporal, and Cell-Type-Specific Profiling of the Murine Cerebral Cortex." *Nature Communications* 15: 2866. https://doi.org/10.1038/s41467-024-46625-w.

Lanjakornsiripan, D., B.-J. Pior, D. Kawaguchi, et al. 2018. "Layer-Specific Morphological and Molecular Differences in Neocortical Astrocytes and Their Dependence on Neuronal Layers." *Nature Communications* 9: 1623. https://doi.org/10.1038/s41467-018-03940-3.

Laug, D., T.-W. Huang, N. A. B. Huerta, et al. 2019. "Nuclear Factor I-A Regulates Diverse Reactive Astrocyte Responses After CNS Injury." *Journal of Clinical Investigation* 129: 4408–4418. https://doi.org/10.1172/JCI127492.

Lee, J.-H., J. Kim, S. Noh, et al. 2021. "Astrocytes Phagocytose Adult Hippocampal Synapses for Circuit Homeostasis." *Nature* 590: 612–617. https://doi.org/10.1038/s41586-020-03060-3.

Leung, V. Y. L., B. Gao, K. K. H. Leung, et al. 2011. "SOX9 Governs Differentiation Stage-Specific Gene Expression in Growth Plate Chondrocytes via Direct Concomitant Transactivation and Repression." *PLoS Genetics* 7: e1002356. https://doi.org/10.1371/journal.pgen.1002356.

Lipovsek, M., C. Bardy, C. R. Cadwell, K. Hadley, D. Kobak, and S. J. Tripathy. 2021. "Patch-Seq: Past, Present, and Future." *Journal of Neuroscience* 41: 937–946. https://doi.org/10.1523/JNEUROSCI.1653-20.2020.

Liu, C., X.-M. Zhao, Q. Wang, et al. 2023. "Astrocyte-Derived SerpinA3N Promotes Neuroinflammation and Epileptic Seizures by Activating the NF-κB Signaling Pathway in Mice With Temporal Lobe Epilepsy." *Journal of Neuroinflammation* 20: 161. https://doi.org/10.1186/s12974-023-02840-8.

Lozzi, B., T.-W. Huang, D. Sardar, A. Y.-S. Huang, and B. Deneen. 2020. "Regionally Distinct Astrocytes Display Unique Transcription Factor Profiles in the Adult Brain." *Frontiers in Neuroscience* 14: 61. https://doi.org/10.3389/fnins.2020.00061.

Malik, T. H. 2001. "Transcriptional Repression and Developmental Functions of the Atypical Vertebrate GATA Protein TRPS1." *EMBO Journal* 20: 1715–1725. https://doi.org/10.1093/emboj/20.7.1715.

Mattugini, N., R. Bocchi, V. Scheuss, et al. 2019. "Inducing Different Neuronal Subtypes From Astrocytes in the Injured Mouse Cerebral Cortex." *Neuron* 103: 1086–1095.e5. https://doi.org/10.1016/j.neuron.2019.08.009.

Nilsson, L. N. G., K. R. Bales, G. DiCarlo, et al. 2001. "α-1-Antichymotrypsin Promotes β-Sheet Amyloid Plaque Deposition in a Transgenic Mouse Model of Alzheimer's Disease." *Journal of Neuroscience* 21: 1444–1451. https://doi.org/10.1523/JNEUROSCI.21-05-01444.2001.

Ohba, S., X. He, H. Hojo, and A. P. McMahon. 2015. "Distinct Transcriptional Programs Underlie Sox9 Regulation of the Mammalian Chondrocyte." *Cell Reports* 12: 229–243. https://doi.org/10.1016/j.celrep.2015.06.013.

Ohlig, S., S. Clavreul, M. Thorwirth, et al. 2021. "Molecular Diversity of Diencephalic Astrocytes Reveals Adult Astrogenesis Regulated by Smad4." *EMBO Journal* 40: e107532. https://doi.org/10.15252/embj.2020107532.

Padmanabhan, J., M. Levy, D. W. Dickson, and H. Potter. 2006. "Alpha1-Antichymotrypsin, an Inflammatory Protein Overexpressed in Alzheimer's Disease Brain, Induces Tau Phosphorylation in Neurons." *Brain* 129: 3020–3034. https://doi.org/10.1093/brain/awl255.

Palomero-Gallagher, N., and K. Zilles. 2019. "Cortical Layers: Cyto-, Myelo-, Receptor- and Synaptic Architecture in Human Cortical Areas." *NeuroImage* 197: 716–741. https://doi.org/10.1016/j.neuroimage.2017.08.035.

Platt, R. J., S. Chen, Y. Zhou, et al. 2014. "CRISPR-Cas9 Knockin Mice for Genome Editing and Cancer Modeling." *Cell* 159: 440–455. https://doi.org/10.1016/j.cell.2014.09.014.

Porter, W., E. Snowden, F. Hahn, et al. 2020. "High Accuracy Gene Expression Profiling of Sorted Cell Subpopulations From Breast Cancer PDX Model Tissue." *PLoS One* 15: e0238594. https://doi.org/10.1371/journal.pone.0238594.

Prakash, P., H. Erdjument-Bromage, M. R. O'Dea, et al. 2024. "Proteomic Profiling of Interferon-Responsive Reactive Astrocytes in Rodent and Human." *Glia* 72: 625–642. https://doi.org/10.1002/glia.24494.

Replogle, J. M., J. L. Bonnar, A. N. Pogson, et al. 2022. "Maximizing CRISPRi Efficacy and Accessibility With Dual-sgRNA Libraries and Optimal Effectors." *eLife* 11: e81856. https://doi.org/10.7554/eLife.81856.

Rowley, C. D., P.-L. Bazin, C. L. Tardif, et al. 2015. "Assessing Intracortical Myelin in the Living Human Brain Using Myelinated Cortical Thickness." *Frontiers in Neuroscience* 9: 396. https://doi.org/10.3389/fnins.2015.00396.

Sadick, J. S., M. R. O'Dea, P. Hasel, T. Dykstra, A. Faustin, and S. A. Liddelow. 2022. "Astrocytes and Oligodendrocytes Undergo Subtype-Specific Transcriptional Changes in Alzheimer's Disease." *Neuron* 110: 1788–1805.e10. https://doi.org/10.1016/j.neuron.2022.03.008.

Sanchez-Gonzalez, R., C. Koupourtidou, T. Lepko, et al. 2022. "Innate Immune Pathways Promote Oligodendrocyte Progenitor Cell Recruitment to the Injury Site in Adult Zebrafish Brain." *Cells* 11: 520. https://doi.org/10.3390/cells11030520.

Sardar, D., H.-C. Chen, A. Reyes, et al. 2022. "Sox9 Directs Divergent Epigenomic States in Brain Tumor Subtypes." *Proceedings of the National Academy of Sciences* 119: e2202015119. https://doi.org/10.1073/pnas.2202015119.

Shibata, A., K. Tanahashi, K. Sugiura, and M. Akiyama. 2016. "TRPS1 Haploinsufficiency Results in Increased STAT3 and SOX9 mRNA Expression in Hair Follicles in Trichorhinophalangeal Syndrome." *Journal of Dermatological Science* 84: e57. https://doi.org/10.1016/j.jdermsci.2016.08.178.

Sirko, S., M. Irmler, S. Gascón, et al. 2015. "Astrocyte Reactivity After Brain Injury—: The Role of Galectins 1 and 3." *Glia* 63: 2340–2361. https://doi.org/10.1002/glia.22898.

Sun, W., A. Cornwell, J. Li, et al. 2017. "SOX9 Is an Astrocyte-Specific Nuclear Marker in the Adult Brain Outside the Neurogenic Regions." *Journal of Neuroscience* 37: 4493–4507. https://doi.org/10.1523/JNEUROSCI.3199-16.2017.

Tan, Z., B. Niu, K. Y. Tsang, et al. 2018. "Synergistic Co-Regulation and Competition by a SOX9-GLI-FOXA Phasic Transcriptional Network Coordinate Chondrocyte Differentiation Transitions." *PLoS Genetics* 14: e1007346. https://doi.org/10.1371/journal.pgen.1007346.

Tiwari, N., A. Pataskar, S. Péron, et al. 2018. "Stage-Specific Transcription Factors Drive Astrogliogenesis by Remodeling Gene Regulatory Landscapes." *Cell Stem Cell* 23: 557–571.e8. https://doi.org/10.1016/j.stem.2018.09.008.

Ung, K., T.-W. Huang, B. Lozzi, et al. 2021. "Olfactory Bulb Astrocytes Mediate Sensory Circuit Processing Through Sox9 in the Mouse Brain." *Nature Communications* 12: 5230. https://doi.org/10.1038/s41467-021-25444-3.

Watson, D. J., G. P. Kobinger, M. A. Passini, J. M. Wilson, and J. H. Wolfe. 2002. "Targeted Transduction Patterns in the Mouse Brain by Lentivirus Vectors Pseudotyped With VSV, Ebola, Mokola, LCMV, or MuLV Envelope Proteins." *Molecular Therapy* 5: 528–537. https://doi.org/10.1006/mthe.2002.0584.

Weng, Q., J. Wang, J. Wang, et al. 2019. "Single-Cell Transcriptomics Uncovers Glial Progenitor Diversity and Cell Fate Determinants During Development and Gliomagenesis." *Cell Stem Cell* 24: 707–723.e8. https://doi.org/10.1016/j.stem.2019.03.006.

Witwicki, R. M., M. B. Ekram, X. Qiu, et al. 2018. "TRPS1 Is a Lineage-Specific Transcriptional Dependency in Breast Cancer." *Cell Reports* 25: 1255–1267.e5. https://doi.org/10.1016/j.celrep.2018.10.023.

Wuelling, M., S. Schneider, V. A. Schröther, C. Waterkamp, D. Hoffmann, and A. Vortkamp. 2020. "Wnt5a Is a Transcriptional Target of Gli3 and Trps1 at the Onset of Chondrocyte Hypertrophy." *Developmental Biology* 457: 104–118. https://doi.org/10.1016/j.ydbio.2019.09.012.

Yang, Y., N. Gomez, N. Infarinato, et al. 2023. "The Pioneer Factor SOX9 Competes for Epigenetic Factors to Switch Stem Cell Fates." *Nature Cell Biology* 25: 1185–1195. https://doi.org/10.1038/s41556-023-01184-y.

Zamboni, M., E. Llorens-Bobadilla, J. P. Magnusson, and J. Frisén. 2020. "A Widespread Neurogenic Potential of Neocortical Astrocytes Is Induced by Injury." *Cell Stem Cell* 27: 605–617.e5. https://doi.org/10.1016/j.stem.2020.07.006.

Supporting Information

Additional supporting information can be found online in the Supporting Information section.